J. Fluid Mech. (1999), *vol.* 383, *pp.* 249–283. Printed in the United Kingdom

Experimental investigations of quasi-two-dimensional vortices in a stratified fluid with source–sink forcing

By FRANS DE ROOIJ, P. F. LINDEN† AND STUART B. DALZIEL

Department of Applied Mathematics and Theoretical Physics, University of Cambridge, Silver Street, Cambridge CB3 9EW, UK

(Received 3 August 1997 and in revised form 13 October 1998)

This paper describes laboratory experiments on the self-organizing character of geophysical turbulence. The experiments were carried out in a linearly stratified fluid, forced horizontally with sources and sinks around a horizontal ring. The flow was visualized with small particles illuminated by a horizontal light sheet, recorded with a camera and analysed with an advanced particle tracking system. Qualitative and quantitative data, such as flow patterns, velocity and vorticity fields, were obtained. In the experiments, the inverse energy cascade was clearly observed: the flow organized into a single quasi-steady, coherent vortex structure of the largest available scale. This vortex is maintained against diffusion of momentum by entrainment of vorticity from its exterior. In this process, patches of vorticity of the same sign as the core of this large structure intermittently cross the vorticity barrier around the vortex. Patches of opposite vorticity were observed to be effectively blocked by the barrier. The direction of rotation of the vortex was set by a slight bias in the experimental apparatus and could be changed by imposing a small initial circulation in the opposite sense, the magnitude of which suggested a measure for the bias. A detailed study of the effects of changing forcing parameters was carried out. The number of sinks (which play only a passive role) does not affect the flow, whereas the number of sources sets the lengthscale of the forcing and thereby determines the size of the vortices that are created close to the ring, as well as that of the large central vortex that emerges. However, after longer times of forcing, the vortex size also depends on the strength of the forcing. The velocities in the large vortex structure scale with the mean velocity from the sources, and with the square root of their number. Measurements were also taken of the decay of the vortex. After switching off the forcing it quickly becomes axisymmetric and a linear functional relationship is established between the vorticity and streamfunction. The spin-down time was observed to be much shorter than can be accounted for by vertical viscous diffusion alone: initially the short horizontal scale of the vorticity barrier causes a relatively fast decay, whereas at later times the size of the vortex as a whole is important.

† Present address: Department of Applied Mechanics and Engineering Sciences, University of California, San Diego, 9500 Gilman Drive, La Jolla, CA 92093-0411, USA.

1. Introduction

The flow in the Earth's atmosphere displays numerous large structures, such as the clockwise and anticlockwise circulations around high- and low-pressure areas. These atmospheric vortices are long-lived and an individual vortex structure can determine the local weather for more than a week. The polar vortex is another strikingly stable feature of the atmospheric circulation. It has had considerable attention in recent years, because of its ozone depletion and the apparent absence of mixing with surrounding air. Some of the planetary atmospheres show similar coherent vortex structures, such as the Great Red Spot on Jupiter.

Satellite observations of the flow in the oceans show that large-scale vortex structures exist there as well. The outflow from the Mediterranean Sea at the Strait of Gibraltar into the Atlantic Ocean is sometimes observed to produce saline eddies at mid-levels, called 'Meddies', that can travel all the way across the Atlantic. Similarly, the meandering Gulf Stream off the coast of Northeast America frequently sheds vortices that can persist for several months.

All these large-scale structures in geophysical circulations have the common characteristic that their flow fields can be regarded, to a good approximation, as two-dimensional in the sense that vertical velocities are much smaller than horizontal velocities. Strictly speaking, the flow is along density surfaces so that the motion is predominantly isopycnal with a very small diapycnal component. The large horizontal scales, compared with the small vertical extent, tend to make the fluid motion approximately planar. The stratification and rotation of the system play an important role in this two-dimensionalization as well. A unique feature of two-dimensional flows is the absence of vortex stretching and twisting, resulting in the so called 'inverse energy cascade'. Energy is transferred to larger scales and a turbulent flow field self-organizes into the coherent structures, such as the stable vortex structures described above.

The inverse energy cascade in two-dimensional flow has frequently been studied using numerical simulations. McWilliams (1984) showed that an initially random distribution of vorticity in a periodic domain organizes into distinct, strong vortices. Numerical studies by Legras, Santangelo & Benzi (1988) and others yielded similar results. Sommeria (1986) showed the emergence of coherent structures in magnetohydrodymanic laboratory experiments. He investigated the flow in a conducting fluid, with turbulence forced by an electric current and making the motions two-dimensional by applying a perpendicular magnetic field. The spectral transfer of energy in a rotating two-layer fluid was studied by Narimousa, Maxworthy & Spedding (1991), applying forcing by surface stress. Yap & Van Atta (1993) also studied the turbulence at the interface between two fluid layers, but forced the turbulence by horizontally traversing a rake of bars. The turbulence from a traversing rake in a continuously stratified fluid was studied by Fincham, Maxworthy & Spedding (1996). Van Heijst and Flór (e.g. van Heijst & Flór 1989; Flór & van Heijst 1994) studied the collapse of three-dimensional jets of finite duration into planar motion and the subsequent organization into dipolar vortex structures in stratified systems. Related laboratory experiments were carried out independently by Voropayev & Afanasyev (1994). This experimental work was extended by Linden and co-workers to continuous forcing with multiple source jets and sinks, in stratified and rotating systems (Boubnov, Dalziel & Linden 1994; Linden, Boubnov & Dalziel 1995; Dalziel, Linden & Boubnov 1996).

The aim of the present work is to obtain a deeper understanding of the emergence and characteristics of coherent vortex structures in a turbulent flow field constrained to be approximately two-dimensional by a stable density stratification. It is an extension

of the earlier work by Boubnov *et al.* (1994) in several aspects. The structure of the vortices and the way they are maintained against diffusion and dissipation are studied in detail. The effects of changing the number of sources and the number of sinks on the evolution of the flow are investigated, as well as the effects of changing their strength. In order to investigate whether a weak bias in the forcing mechanism sets the direction of the final circulation, a separate series of experiments was carried out to study the effects of an initial perturbation on this direction. Finally, measurements were taken of the decay of the vortices when the flow was no longer forced, and allowed to spin down.

The format of this paper is as follows. The set-up of the experiments is described in the next section. In § 3 the structure of the circulation is discussed, in § 4 the effects of different forcing parameters are described, in § 5 the effects of an initial perturbation are examined and in § 6 the decay of the circulation when the forcing is switched off is discussed. The last section contains the conclusions.

2. Experiments

The experiments described in this paper were carried out with largely the same experimental equipment as used by Linden *et al.* (1995). A concise description will now follow.

A rectangular Perspex tank with horizontal inside dimensions of $61.0 \times 61.0\,\mathrm{cm}^2$ and a height of 44.5 cm was carefully filled via a porous raft to a level H of 22 cm with a vertically stratified salt (NaCl) solution using a double-bucket system. The same strength of stratification was used for each experiment. The linear density stratification was sampled at several levels. A least-squares fit to these data yielded a gradient $\rho^{-1}(\partial\rho/\partial z)$ of approximately $-0.08\,\mathrm{m}^{-1}$, corresponding to a buoyancy frequency N of $0.9\,\mathrm{s}^{-1}$.

A circular Perspex ring was suspended horizontally in the tank at a height 11.3 cm above the bottom. The ring had an inside diameter of 56.3 cm and a thickness of 10 mm. Its vertical inner face contained 80 radially directed orifices with a diameter d of 0.40 cm. Each of these holes was connected to a small vertical pipe, that could be connected via flexible tubing to an eight-channel peristaltic pump. The flow produced is pulsating with the velocities varying by approximately 50% at a frequency of 2–6 Hz, depending on the pump speed. However, related experiments (A. L. Kurapov, private communication) indicated that the effects of these pulsations are negligible and the results will only be discussed in terms of the mean velocities from the sources. By using flow dividers various numbers of sources and sinks were created, sucking out fluid and injecting it at the same level (see figure 1). The source jets are all directed radially inward with the intention that no net momentum or angular momentum is imparted to the fluid. A range of different active source–sink configurations were used in the experiments. In each case the forcing had min (m, n)-fold rotational symmetry about the centre of the tank, where m, n is the number of sources and sinks (respectively) in use. The lengthscale of the forcing l was defined as the equal circumferential spacing between the sources.

To visualize and quantify the flow, the tank was seeded with small white particles, made by grinding pliolite VTAC, a brilliant white opaque resin used in the manufacture of solvent-based paints. Via subsequent sieving the particles with a diameter d_p of 0.5–0.6 mm were selected. The ratio between the convective force and the drag on the particles is expressed by the dimensionless Stokes number $St = V d_p^2/(18\nu\, l)$, where V and l are the characteristic velocity scale and lengthscale of the surrounding

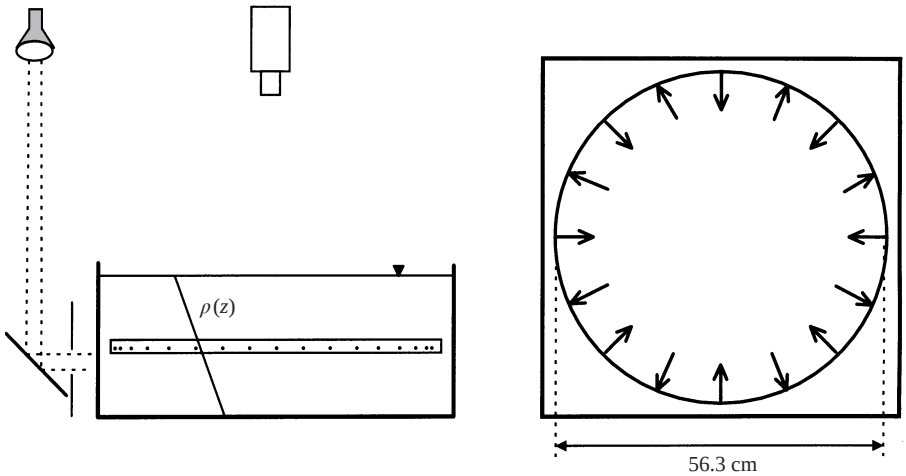

FIGURE 1. Elevation and plan view of the experimental set-up. The source/sink locations indicated at the forcing ring are those used in the experiments with 8 sources and 8 sinks. Both these numbers could be varied.

flow and v the kinematic viscosity. In the present work $St \approx 0.004$, so the velocity of the particles is, to a good approximation, equal to the local flow velocity. The density stratification in the tank was chosen in such a way that the particles, with an average density of $1.025 \times 10^3\,\mathrm{kg\,m^{-3}}$, were neutrally buoyant at the level of the ring with the sources and sinks. The narrow distribution of particle densities meant that the particles were vertically spread over approximately 3 cm. To illuminate the particles a horizontal light sheet with a thickness of 5 mm was set up just below the ring, using two slide projectors and mirrors on opposite sides of the tank. The top of this light sheet was only 3 mm below the centre of the orifices and the motion induced by the forcing is tracked well with the illuminated particles.

After filling the tank and adding the particles, the pump was run for several minutes to clear the air from the tubing. Several hours then elapsed before an experiment was started, to minimize any residual circulation. The pump speeds used in the experiments were in the range 24–94 revolutions min^{-1}, yielding, with numbers of sources and sinks of either 8 or 16, a mean velocity V from the sources between 1.59 and $3.19\,\mathrm{cm\,s^{-1}}$. Owing to differences in length and connections of the tubing and the blocking effect of some persistent air bubbles, differences in the mean velocity from the individual sources occur. From measurements of the volume flux from the 8 sources, the standard deviation of the mean velocity was estimated to be 2%. Where flow splitters were used to create 16 sources, larger differences in flow speeds occurred. They could not practicably be measured in this case, but are estimated to be around 10% and may range upwards to 30%.

The horizontal motion of the particles was recorded with a CCD video camera, mounted 1.3 m above the centre of the tank, on a super-VHS tape recorder for up to 4 hours after the start of the forcing. A computer system with a frame-grabber card and the image processing software DigImage was used for the off-line processing of the recordings. Typically, about 1200 particles were tracked in the video frames, acquired at time intervals of 0.2 s. The further details of the particle tracking software have been described by Dalziel (1992, 1993). The velocity field was obtained by mapping the individual particle velocity vectors onto a rectangular grid using spatial

averaging over 1.5 cm with a triangular weighting function. Derived quantities such as the vorticity and streamfunction were calculated from these gridded velocity data for every mesh between four grid points. The arbitrary constant in the definition of ψ is chosen to yield an average ψ value of zero over the whole field. The error in the velocities and streamfunctions was estimated by Dalziel (1993) to be 5%, whereas the error in the other derived fields is probably 10%.

The first series of experiments investigated the response to different forcing velocities and lengthscales and to different arrangements of sources and sinks. The evolution of the flow was studied in detail in experiments where the flow was forced with 8 sources and 8 sinks. Following this, experiments were carried out with a doubled number of sources or sinks. This was achieved by connecting either the sucking or the pumping side of each pump channel to two of the orifices in the forcing ring instead of one. The experiments with 8 sources and 8 sinks and with 16 sources and 8 sinks were repeated at several different forcing strengths.

The second series of experiments was performed with a perturbation present before the forcing was started to determine the sensitivity of the direction of the final circulation to the initial conditions. This small initial flow was induced by rotating the tank clockwise at a slow speed (0.02 rad s^{-1}) over 90° and consequently allowing some time (10–40 min) to let the flow become more axisymmetric and decay to the desired strength, before starting the forcing.

The third aspect was to observe the spin-down of the vortex after the forcing was turned off. In some experiments a more elliptical vortex structure was created by disconnecting four of the pump channels 1 hour before the switch-off, and the evolution towards a circular flow was observed.

Several non-dimensional numbers can be constructed to characterize the behaviour of the flow. The Reynolds number based on the diameter of the sources $Re_d = Vd/\nu$ was around 100, indicating that the flow from the sources was laminar and little small-scale turbulence is injected. However, the Reynolds number based on the lengthscale of the forcing l yields values for $Re_l = Vl/\nu$ of 1700–4000, so the flow produced by the forcing as a whole can be regarded as turbulent. The strength of the forcing relative to the stratification can be expressed with the forcing parameter $F_l = V/Nl$, which has the form of a Froude number. Again, the source spacing l rather than the orifice diameter d is used to characterize the flow away from the sources. At large values of F_l the flow from the sources produces strong vertical mixing, but the present experiments were restricted to low jet speeds. Values of F_l were around 0.15, corresponding to values of the forcing parameter based on the orifice diameter F_d of 4–9. Some vertical mixing was observed, but the forcing was weak enough to make the flow collapse into planar motion. This matches the observations by Boubnov *et al.* (1994), who noted in this parameter range a transition from regime I (vortex interaction) to regime II (large-scale circulation).

The flow may also depend weakly on the Péclet number, defined by $Pe = Vl/\kappa$. The relevance of this dependency is characterized by the Prandtl number $Pr = \nu/\kappa$, giving the relative importance of viscosity and molecular diffusion, which has a value of 6×10^2 in these experiments. This large value indicates that the dependence on the Reynolds number of the flow is larger than that on the Péclet number, but the dependence on the Reynolds and Péclet numbers is believed to be weak and will not be considered further here. Table 1 gives data on the experiments used in the analysis of this paper.

Exp.	Number of sources/sinks	V (cm s^{-1})	N(s^{-1})	F_l	Re_l
5	16/8	1.59	0.96	0.151	1757
6	8/16	3.19	0.93	0.156	7053
7	8/8	3.19	0.94	0.153	7053
8	8/8	3.19	0.90	0.161	7053
16	16/8	2.24	0.95	0.205	2475
17	16/8	2.53	0.94	0.243	2796
18	16/8	3.19	0.90	0.323	3525
19	16/8	2.24	0.91	0.214	2475
20	8/8	1.63	0.95	0.077	3604

TABLE 1. Parameters for the experiments described in the text. Experiments indicated in the text by a number plus a lower case letter have identical parameters to the experiment with the same number.

3. Structure of the circulation

3.1. *Observations*

The set-up and parameter regime of the non-rotating experiments with 8 source–sinks pairs carried out by Linden *et al.* (1995) were identical to the experiments described in this section. The sources produce three-dimensional jets, inducing a small amount of vertical mixing that was studied in more detail by Boubnov *et al.* (1994). However, at the low values of the forcing parameter F_l used, the vertical motion is quickly suppressed by the density stratification and the flow becomes planar. The source jets produce a vortex cylinder, that collapses into a double vortex strip, with negative vertical vorticity to the right of the jet and positive to the left. These vortex strips roll up to form vortex dipoles that penetrate into the interior of the tank, where they interact. The initially irregular vorticity distribution in the interior of the tank self-organizes into one large positive axisymmetric vortex (see figures 2 and 3). This organization is consistent with the inverse energy cascade law for two-dimensional turbulence. The vortex occupies a large central area in the tank, leaving only an exterior region a few centimetres wide where the influence of the individual sources and sinks is important. At early times, the motion is still vertically confined to levels close to the forcing, but this vertical shear is slowly reduced and some motion can be observed at the surface (11 cm above the forcing ring) approximately 15 min after the start of the forcing. We believe the three-dimensional effects are relatively small, unlike the experiments of Fincham *et al.* (1996) where the forcing throughout the whole fluid depth led to interaction between vortices at different levels.

In the present experiments, we will look in more detail at the structure of the large-scale circulation and the way it is maintained. In the quasi-steady state, the vorticity of one sign is concentrated in a regular pattern of vortices around the ring, with a size set by the spacing of the sources. Vorticity of opposite sign is accumulated in the large vortex in the interior of the tank and becomes axisymmetric after 10–15 min, corresponding to non-dimensional times $Nt \approx 10^3$.

The dominating central vortex was observed to be strengthened by entrainment of patches of vorticity coming directly from the sources. An example of this can be seen in the sequence of flow fields displayed in figure 2. In figure 2(*a*), a small but strong positive vortex is present, close to the source on the left-hand side of the tank at the 9 o'clock position, indicated by the large arrow. After 20 s (figure 2*b*) the separate

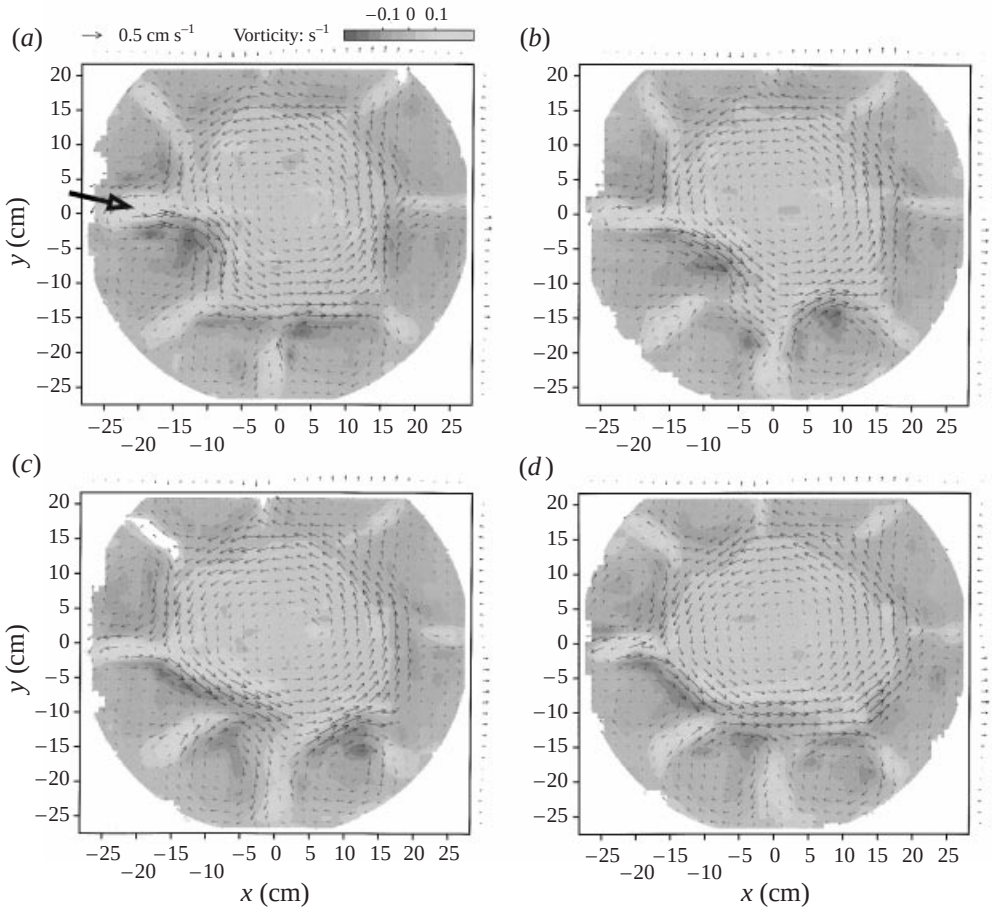

FIGURE 2. Velocity and vorticity fields in Exp. 7 indicated by the arrows and the shading, respectively, at (*a*) 11′40″, (*b*) 12′00″, (*c*) 12′20″ and (*d*) 12′40″ after the start of the forcing. The large arrow points at the concentrated positive vortex produced by one of the source jets, and its evolution is further described in the text. Forcing by 8 sources and 8 sinks at the locations indicated in figure 1, with $V = 3.2$ cm s^{-1}.

circulation in that small vortex has linked up with the circulation in the large central vortex, providing a flux of positive vorticity into the central vortex. The negative vorticity produced by the same source jet does not penetrate into the interior, but merges with the clockwise vortices at 7 and 8 o'clock (figure 2*c*). In figure 2(*d*) we see that the source vortex has a circulation that is separate from the central circulation again. This process repeats at other locations around the forcing ring.

Observations of the particle trajectories (figure 3) also show that the flow exhibits unsteady behaviour. All particle trajectories longer than 3 s are plotted. The trajectories have lengths up to 9 s, comparable with the timescale of the forcing $l/V \approx 7$ s, but quite short compared with the circulation time of the central vortex $T_c = \pi D/U_{max} \approx 180$ s. Here D is the diameter of the central vortex and U_{max} the maximum velocity measured at its edge. Unfortunately, the length of the trajectories could not be improved in the current experimental set-up as, owing to a combination of signal noise, the small size of the particles and weak vertical motions, a significant fraction of the particles would disappear or appear to become too small to track reliably.

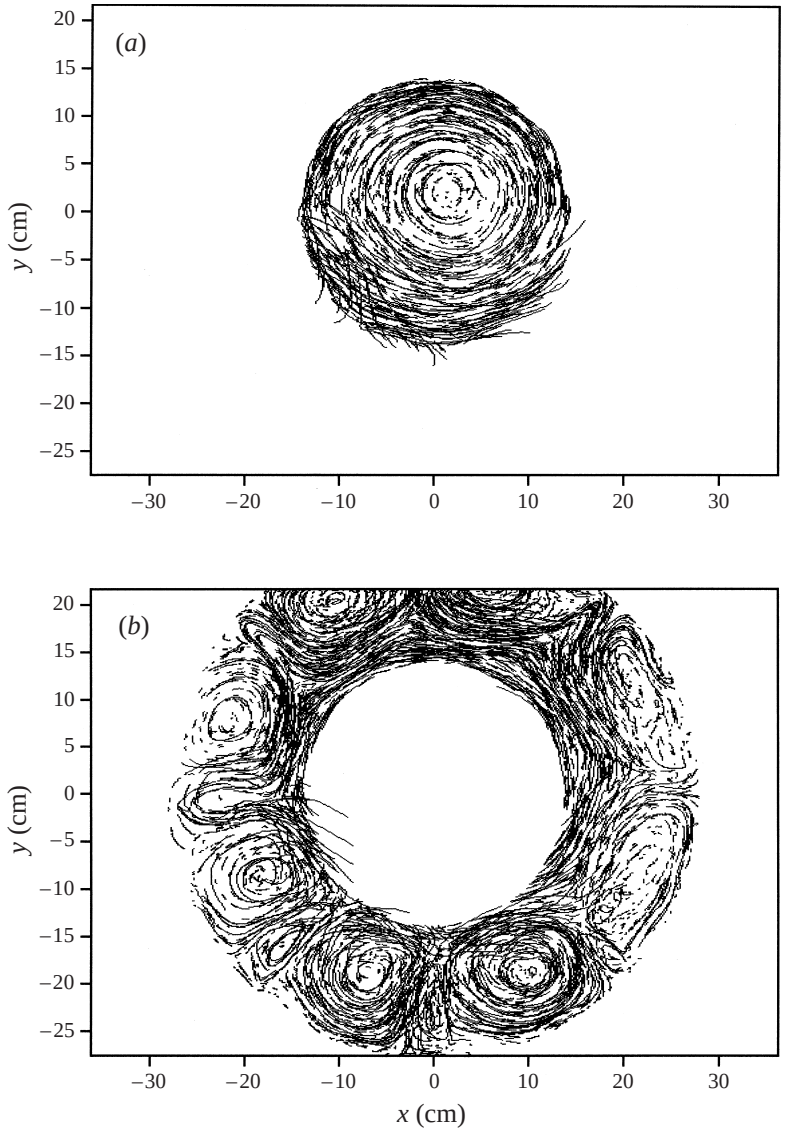

FIGURE 3. Particles traces accumulated from 11′30″ until 14′00″ after the start of the forcing in Exp. 7. Only traces with a length longer than 3 s are displayed. Traces started in the central area of the domain with (*a*) $r < 14$ cm, and in the ring around this with (*b*) $14\,\text{cm} < r < 28\,\text{cm}$.

Figure 3(*a*) shows that the vast majority of trajectories in the central area have the form of a section of a circle, indicating closed streamlines within the central vortex. Only a small number of the trajectories that start from the central vortex (which is rotating in the anticlockwise direction) break out and end up in a source vortex, as we see at 4 and 5 o'clock. Similarly, most particles starting in the outer region stay in one of the smaller vortices linked to the sources (figure 3*b*). Occasionally, a small amount of fluid from one of the sources becomes entrained into the central vortex. The event shown in figure 2 and described above is a good example of this. The same event is indicated in figure 3(*b*) by the streaks from the ring into the centre at 9 o'clock. The patch of negative vorticity that is advected from one of the source

vortices towards the centre and consequently expelled again, is traced by the particles entering the centre at 8 o'clock in figure 3(*b*) and leaving again at 7 and 6 o'clock in figure 3(*a*).

We should note that, since the central circulation remains constant in size, in the mean there must be as much fluid leaving the central vortex as entering it. There is, however, an asymmetry in the momentum and vorticity fluxes associated with entering and leaving events. As we shall see later, fluid entering the central circulation has, in the mean, a larger vorticity than the central circulation, while fluid leaving it has a lower vorticity. Evidence of this asymmetry of the vorticity flux was found by Boubnov *et al.* (1994).

Figure 4 shows cross-sections of the velocity and the vorticity fields at the times when the quasi-steady state is first reached (figure 4*a*) and when the flow has been quasi-steady for a long time (figure 4*b*). The plots do not differ qualitatively. In the middle region of the flow, the vorticity is approximately constant and correspondingly the velocities increase linearly with radius. Higher vorticity values occur at the outer edge of the central vortex, followed by large negative vorticity values in the ring of surrounding vortices. This gives a band of slightly higher velocities around the vortex. The mean value of the vorticity is close to zero, as expected since the velocities vanish at the wall, and hence the circulation around the tank perimeter is zero.

Figure 5 shows scatter plots in the (ω, ψ)-plane at the same times as the cross-sections in figure 4. Here ψ represents the streamfunction for the velocities (u, v) in a horizontal plane, and ω the vertical component of the vorticity. All points within the flow in physical space are plotted in (ω, ψ)-space. The streamfunction ψ has its maximum in the middle of the anticlockwise circulation of the positive central vortex. Decreasing values of ψ correspond to increasing distances from the centre. Since the definition of ψ was chosen to yield an average value of zero over the whole field, the parts of the plots with negative ψ correspond to the areas outside the central vortex.

The approximately constant value of the vorticity at positive values of ψ in figure 5(*a*) indicate once more a homogeneous distribution of vorticity in the interior of the central vortex. Slightly higher vorticities occur at the edge of the vortex, especially at later times (figure 5*b*). The negative vorticity is concentrated at the outside of the domain, close to the forcing ring. The amount of scatter here is greatly reduced at later times, indicative of a more organized flow.

To estimate the quantitative fluxes across the region with high velocities into the central vortex we use a diagnostic technique first described by Read, Rhines & White (1986). They showed that the net flux of vorticity out of a closed loop in physical space is equal to the area enclosed by the corresponding circuit in (ω, ψ)-space. For a stationary, strictly two-dimensional flow without viscosity, the vorticity is a function of streamfunction: $\omega = \omega(\psi)$. Any departure from this functional relationship will give rise to a non-zero enclosed area in (ω, ψ)-space, representing a vorticity flux across streamlines.

Figure 6 shows an (ω, ψ)-plot for a centred circle with radius 12 cm in the flow field of Exp. 7. This circle is inside and close to the edge of the large vortex. The hatched areas indicate a flux of positive vorticity into this circle. Most of the entrained vorticity is stronger than the average vorticity in the vortex, and only a negligible amount of negative vorticity is entrained. The dotted areas represent outward fluxes of positive vorticity, and these can be seen to be much smaller than the inward fluxes. By integration, the net flux Φ into the central area was calculated to be $9 \times 10^{-3}\,\mathrm{cm^2\,s^{-2}}$, which corresponds to a relative increase rate of the average vorticity $\bar{\omega}$ in the enclosed

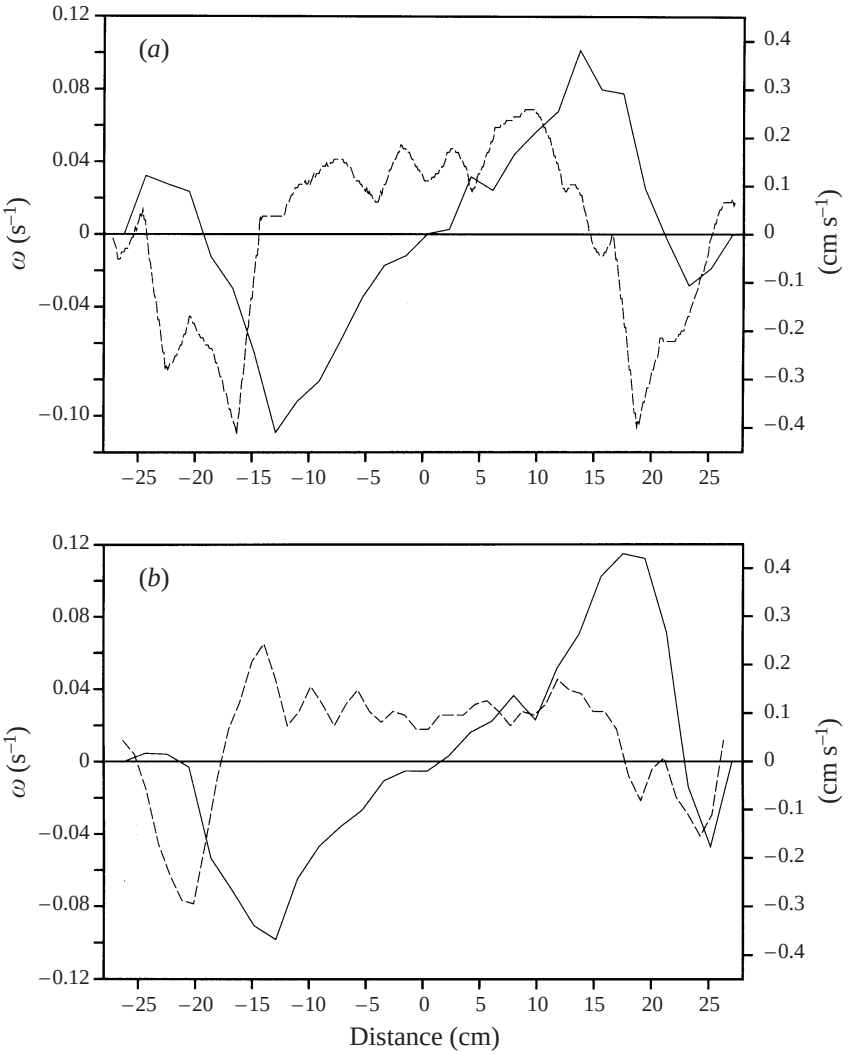

FIGURE 4. ——, Perpendicular velocities and - - -, vorticity values on the line $y = -\frac{1}{2}x$ in Exp. 7, with x and y as in figure 3. (*a*) 13 min and (*b*) 90 min after the start of the forcing.

area of

$$\frac{1}{\bar{\omega}}\frac{\partial \bar{\omega}}{\partial t} = \frac{1}{\bar{\omega}}\frac{\Phi}{\pi r^2} \approx 3 \times 10^{-4}\ \mathrm{s}^{-1}. \tag{1}$$

The vorticity flux into the central area is plotted as a function of time in figure 7. At early times, before the coherent central vortex appears, the flux exhibits large fluctuations. The time-resolution of this figure is somewhat low, but detailed analysis of a much shorter interval showed that both amplitude and frequency of the fluctuations are well characterized by this figure. After the central vortex has appeared, the flux across a circle with a radius of 12 cm becomes, on average, positive. The flux across a circle with a radius of 14 cm, coinciding more or less with the band of high velocities at the boundary of the central vortex, still fluctuates sharply at later times. These fluctuations for the 14 cm radius are largely due to the motion of the vortex boundary, rather than actual vorticity entrainment by the central vortex.

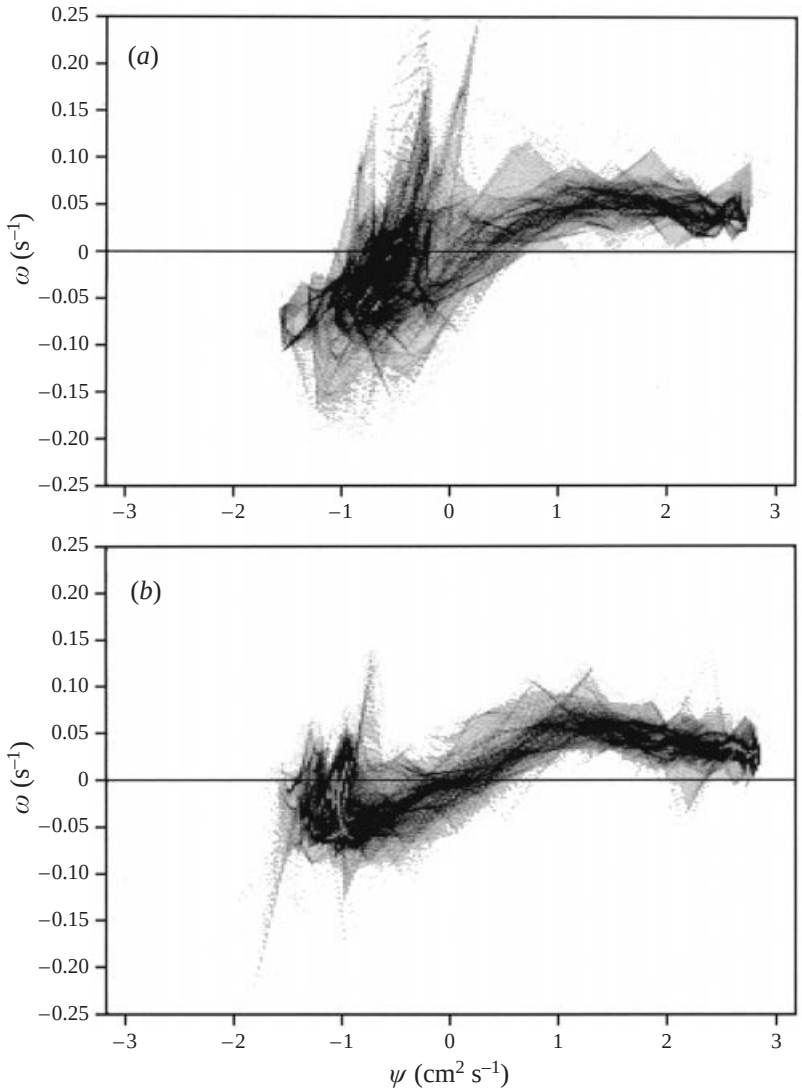

FIGURE 5. (ω, ψ) scatter plots of the vorticity field in Exp. 7 during spin-up, at (*a*) 13 min and (*b*) 90 min after the start of the forcing. The (ω, ψ)-values of all points on a grid in physical space, with a mesh size of approximately $(1\,\mathrm{mm})^2$, are plotted.

3.2. *Discussion*

As can be seen from the cross-sections in figure 4 and the scater plots in figure 5, the vorticity is almost constant over the central area of the vortex, with an average value of approximately 0.04 s^{-1}. After forcing for a long time, the vorticity in the centre remains unchanged, while the vorticity close to the edge of the vortex has increased, yielding values up to 50% higher. Combined with the ring of strong negative vorticity near the forcing ring, this results in a rapid radial decrease in the vorticity just outside the large-scale circulation, where the velocity is maximum.

The thin region of large vorticity gradients results in a vorticity barrier or 'eddy-transport barrier', that shields the central circulation. This phenomenon is of particular relevance to atmospheric dynamics and has been the subject of many recent investi-

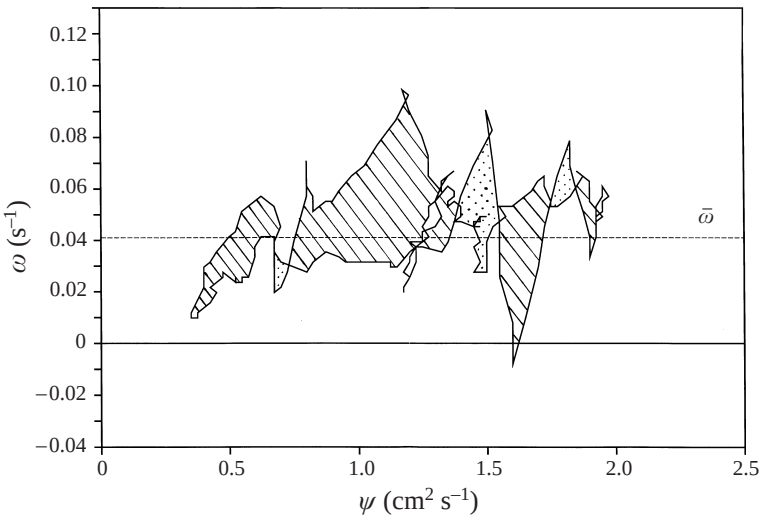

FIGURE 6. Representation in (ω, ψ)-space of a circle with 12 cm radius centred in the flow field of Exp. 7, 13 min after the start of the forcing. When the physical circle is traced in a counterclockwise direction, the hatched areas are encircled in a counterclockwise sense and the dotted areas in a clockwise sense, indicating inward and outward fluxes, respectively. - - -, average value of the vorticity in the central area.

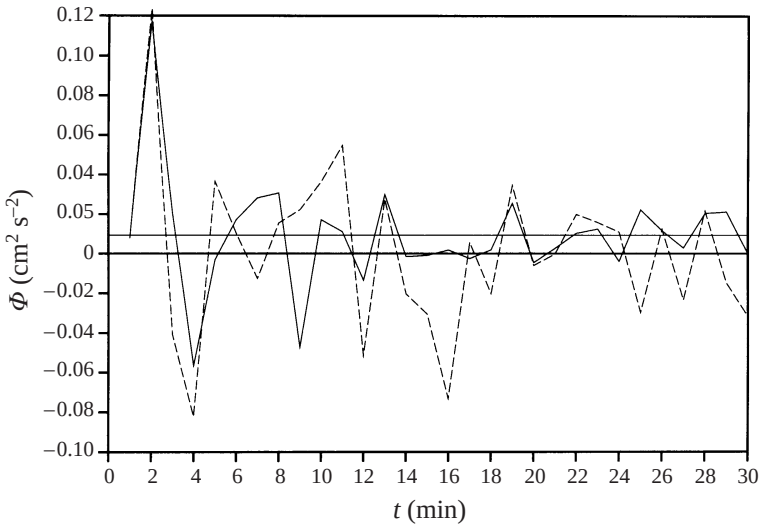

FIGURE 7. Time-evolution of the net vorticity flux Φ into the central area, calculated from (ω, ψ)-plots as in figure 6. ——, flux across a circle with 12 cm radius; - - -, flux across a circle with 14 cm radius. The 30 min time-average of the former is indicated by the horizontal line.

gations using numerical simulations (see e.g. Norton 1994 and references therein). It is believed that the negative shear around a large positive vortex effectively provides an elastic barrier to negative vortices, whereas positive vortices will be able to approach the large vortex and eventually become wrapped around it.

Careful observation of our experiments, in particular the time-evolution shown in figures 2 and 3, indicates that a patch of negative vorticity initially moving towards the centre was indeed reflected by the vorticity barrier, and finally drawn into the

negative vortices at the sources. On the other hand, patches of positive vorticity from the sources are observed to cross the barrier intermittently. This corresponds closely to the results of the numerical simulations by Dritschel, Haynes & McIntyre (1998) for a vortex dipole approaching a large vortex. In our experiments, the positve vorticity advected into the central circulation is subsequently spread out by horizontal diffusion.

The circulation in the central vortex will decay with time, unless it is maintained against viscous dissipation. It can be shown that the horizontal diffusion of momentum is much too small to maintain a central circulation of this magnitude and form. Unsteadiness of the flow and horizontal advection of vorticity provide the mechanisms to balance the diffusive and disssipative effects. The time-evolution of the experiments (figures 2 and 3), as well as the observed deviations from the functional relationship $\omega = \omega(\psi)$ (shown in figure 6), show that the edge of the vortex is unsteady. The enclosed area in the ω–ψ plot signifies a dominant inward flux of positive vorticity, resulting from the entrainment of positive vorticity and the expulsion of negative vorticity by the vorticity barrier, as described above.

We compare quantitatively the flux of vorticity into the central vortex with a decay model recently described by Flór & van Heijst (1996) for monopolar vortices. We consider only viscous spread of vorticity, leaving out the contribution by advection or any effects of internal waves. Assuming no tilting or twisting of vortex lines is present, and therefore no three-dimensional dissipational effects, we can write down the equation for the diffusion of the vertical component of the vorticity as

$$\frac{\partial \omega}{\partial t} = \nu \frac{\partial^2 \omega}{\partial z^2} + \nu \nabla_h^2 \omega. \tag{2}$$

Visual observation of the flow suggests that the horizontal velocities drop from their maximum value at the level of the sources to less than a third of the maximum approximately 3 cm above and below that plane, indicating a similar vertical gradient in the vorticity. The cross-sections in figure 4 show that horizontally the vorticity changes from its maximum to its minimum value at the edge of the central vortex in approximately 6 cm. This implies that the typical horizontal and vertical vorticity gradients are roughly comparable. At the edge of the vortex, we expect horizontal diffusion to play a small role compared to the horizontal advection of vorticity, and as a further approximation we neglect the last term in (2). We assume a Gaussian vorticity profile in the vertical, with a constant characteristic spread of σ during a short time interval. From this, we obtain the solution for the vorticity in the central vortex at levels close to the forcing ($z/\sigma < 1$) as

$$\omega(r, z, t) = \omega(r) \exp\left(-\frac{z^2}{2\sigma^2}\right) \exp\left(-\frac{t}{\tau}\right), \tag{3}$$

where the characteristic timescale for vertical viscous diffusion is $\tau = \sigma^2/\nu$. This gives a relative decay rate at the level of the forcing of

$$-\frac{1}{\omega}\frac{\partial \omega}{\partial t}\bigg|_{z=0} = \frac{1}{\tau} = \frac{\sigma^2}{\nu}, \tag{4}$$

a result which still holds when we take a spreading Gaussian distribution in the vertical with $\sigma = \sigma(t)$. Observations of the vertical spread of horizontal motion in the present experiments suggest $\sigma = 3$ cm as an estimate for the vertical extent of the flow at $Nt \approx 800$, giving a timescale of 15 min and a relative decay rate of the order of 10^{-3} s^{-1}. Thus, the vertical viscous diffusion of vorticity is of the same magnitude as the measured vorticity increase rate due to horizontal advection (1). This suggests that

Exp.	Number of sources/sinks		Velocity V	Volume flux $Q = nAV$
7	8/8	Reference	V_0	Q_0
20	8/8	Halved forcing velocity	$2^{-1}V_0$	$2^{-1}Q_0$
6	8/16	Equal volume flux $Q = nAV$	V_0	Q_0
5	16/8	Equal volume flux $Q = nAV$	$2^{-1}V_0$	Q_0
19	16/8	Equal momentum flux $M = n\rho AV^2$	$2^{-1/2}V_0$	$2^{1/2}Q_0$
17	16/8	Equal energy flux $E = n\rho AV^3$	$2^{-1/3}V_0$	$2^{2/3}Q_0$
18	16/8	Equal jet velocity V	V_0	$2Q_0$

TABLE 2. Summary of the experiments.

the observed more or less constant strength of the central vortex can be accounted for by a vorticity balance between vertical viscous diffusion and horizontal advection.

Another point worth noting is that in a strictly two-dimensional flow with no viscosity, the vorticity of a fluid element is always constant owing to the absence of vortex intensification by stretching. The largest value of the vorticity crossing the closed loop around the central vortex therefore poses a maximum to the vorticity in its interior. Observed maximum values of 0.1 s^{-1} crossing the circle with $r = 12$ cm (figure 6) are well above the measured vorticities within it. Since enstrophy cascades to smaller scales we do not expect the vorticity elements to accumulate in such a way as to generate velocities greater than the initial forcing velocity. The observed maximum peak velocity of approximately 0.53 cm s^{-1}, occurring at the edge of the central vortex, is 17% of the mean velocity from the sources V.

4. Dependence on number and strength of sources and sinks

4.1. *Observations*

In order to investigate the differences between sources and sinks on the evolution of the flow, a series of experiments was carried out with a doubled number of either sources or sinks. The total strength of the forcing was also varied. Experiments were performed where, with respect to the reference experiment, the total volume flux, momentum flux, energy flux or the jet velocity was kept constant. Table 2 provides a summary of the experimental parameters, where A is the area of a source orifice, n is the number of sources and V is the velocity from the sources.

The time-evolution and the final state properties of the reference experiment (Exp. 7) were described in § 3.1.

The results of Exp. 6 showed that doubling the number of sinks, keeping the total volume flux constant, induced only small changes to the flow. The flow still has the same 8-fold symmetry as the sources. In the early stages of the flow evolution, the heads of the vortex strips emerging from the sources are slightly more dispersed, but they penetrate into the interior of the tank in the same way and upon interaction a disordered vorticity distribution arises. The consequent development of a large-scale circulation remained qualitatively unchanged; the positive vorticity accumulates into one vortex that slowly grows in size and becomes quasi-steady and approximately axisymmetric at non-dimensional times $Nt > 10^3$. This final state is qualitatively identical to the final state reached in the experiment with only 8 sinks.

In the early stages ($Nt < 100$) in all experiments, the velocities show a rapid

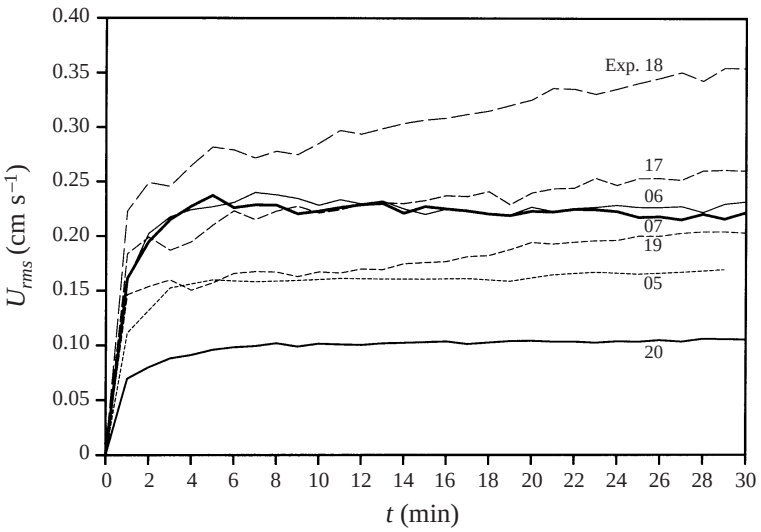

FIGURE 8. The time-evolution of the r.m.s. velocity of the experiments listed in table 2. The data are based on the velocities of all tracked particles in the field, averaged over 4 s.

acceleration as the motion from the sources penetrates into the interior. Figure 8 shows the evolution of the root-mean-square velocity U_{rms} averaged over the whole field for the experiments listed in table 2. Comparison of the experiments that only differ in the number of sinks (Exps. 6 and 7) shows that they are also quantitatively very similar. The constant velocity reached after $Nt \approx 300$ is, within the experimental error, the same in these two experiments.

A reduction of the forcing velocity, as studied in Exp. 20, had no noticeable effects on the qualitative time-evolution of the flow, nor on the shape of the final state. Quantitatively, the timescale for the large-scale circulation to develop was somewhat longer, and the strength of the circulation was weaker. We compare the velocities by the triangular markers in figure 9, representing the two experiments with 8 sources (Exps. 20 and 7). The two open markers for U_{rms} for the fully established flow ($Nt > 2.10^3$) collapse onto the dash-dotted line, a least-squares fit to the data forced to go through the origin. Similarly, the two solid markers for the maximum velocity U_{max} in the final state collapse onto the solid line. This indicates that both U_{rms} and U_{max} scale linearly with the jet velocity V. Furthermore, the maximum velocity is approximately twice as large as the r.m.s. velocity.

In the experiments with the doubled number of sources (Exps. 5, 17, 18 and 19), some important differences compared with Exp. 7 in the evolution of the flow were observed. The reduction in the forcing lengthscale clearly decreases the scale of the initial dipoles from the sources, as can be seen by comparing figures 2 and 10. This was also observed by Linden *et al.* (1995) in their experiments with 20 and 40 source–sink pairs. Consequently, the heads of the vortex strips do not propagate all the way to the middle of the tank, but start interacting closer to the sources. In the early stages of the evolution (figure 10*a*) we observe 32 small vortices of alternating sign around the forcing ring. The 16 sources determine this flow pattern to a large extent, although, formally, the flow only has 8-fold symmetry because of the smaller number of sinks. This gives rise to small differences compared with the experiments with a reduced forcing scale by Linden *et al.* (1995). We observed that the 16 clockwise

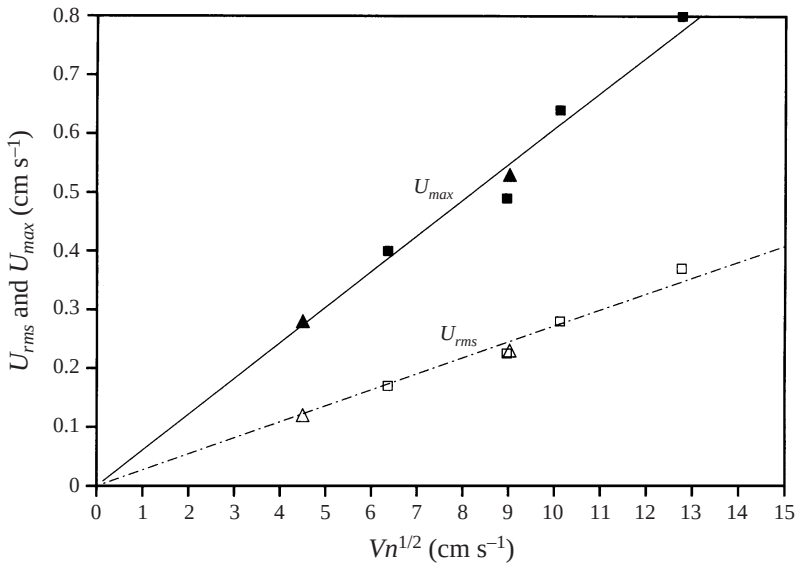

FIGURE 9. Measured velocities in the fully evolved fields ($t > 25$ min) of the experiments listed in table 2. Maximum velocity (defined as the velocity only exceeded by 1% of the trajectories) and r.m.s. velocity (averaged over all trajectories in the field) plotted against the forcing velocity V multiplied by the square root of the number of sources n. ▲ and △, experiments with a forcing with 8 sources; ■ and □, forcing with 16 sources.

vortices around the ring do not have the same strength: the ones that are located between two sources without a sink in between tend to be well pronounced, whereas some vortices located in front of a sink orifice are hardly visible.

Somewhat later, the positive vorticity tends to spread out into the interior of the tank, while the negative vortices stay closer to the ring (see figure 10*b*). A few flow structures appear in the interior of the tank, but they are less organized and on a smaller scale than in the experiment with 8 sources. Subsequently, these, mainly positive vorticity structures, evolve into one large vortex, as described before. The quasi-steady final state shows a central vortex with a much larger extent than in Exp. 7, and the vortices around the ring are smaller. These small vortices still have small differences in strength, depending on the proximity of a sink. The time it takes for the central circulation to become approximately axisymmetric is comparable for almost all experiments ($Nt \approx 10^3$), and differences in the strength of the forcing had no qualitative effect on the time-evolution of the flow. Only in one of our experiments (Exp. 16) was a different evolution observed: two large vortices of opposite sign persist in the centre for a very long time. This is most probably a result of an inequality of the forcing jets caused by air bubbles trapped in the tubing after the flow dividers, but even in this experiment the flow eventually became axisymmetric.

We now return to figure 8 and compare the time-evolution of Exps. 5, 17, 18 and 19 quantitatively with the reference Exp. 7. All the curves have approximately similar shapes, but differences occur in the timescales of the spin-up. After 10 min, U_{rms} has become approximately constant in the experiments with 8 sources. In the experiments with 16 sources this takes longer: up to 25 min. During the early upscaling process ($Nt < 10^3$) the experiment with the same energy (Exp. 17) shows approximately the same evolution as the reference experiment. After the flow has become axisymmetric the r.m.s. velocity in Exp. 17 still increases a little, while the experiment with equal

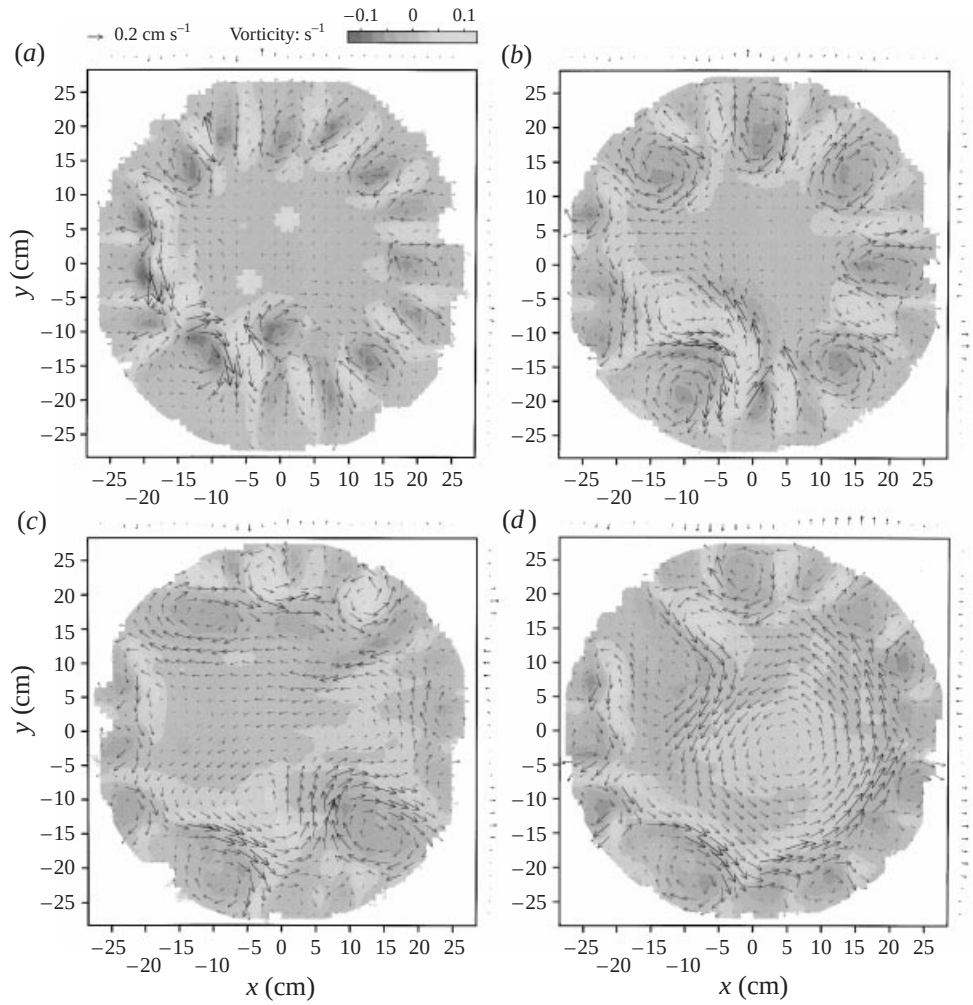

FIGURE 10. Plots of the velocity and vorticity in Exp. 19. The flow was forced with 16 sources and 8 sinks, with $V = 2.24$ cm s^{-1}. The 8 sinks were positioned as indicated in figure 1, and the 16 sources are positioned equidistantially between these. Times after the start of the forcing: (*a*) 1 min, (*b*) 2 min, (*c*) 4 min, (*d*) 8 min.

momentum flux (Exp. 19) resembles the reference experiment better; the velocities in the final state are approximately the same.

Since all other parameters were kept constant in these experiments, the final velocity can only depend on the source velocity V and the number of sources n. The observed velocities U_{rms} and U_{max} in the fully developed flow are plotted in figure 9 versus the mean source velocity V. The square markers that represent the experiments with 16 sources (Exps. 5, 19, 17 and 18) collapse onto straight lines, indicating that the velocities in the flow scale with the jet velocity. The plot also shows that the additional scaling with the square root of the number of sources $n^{1/2}$ collapses the experiments with 8 sources and with 16 sources onto the same lines. The markers for Exp. 19 even coincide (within the experimental error) with the ones for the reference experiment. This linear dependence of the observed velocities on the parameter $Vn^{1/2}$ can be

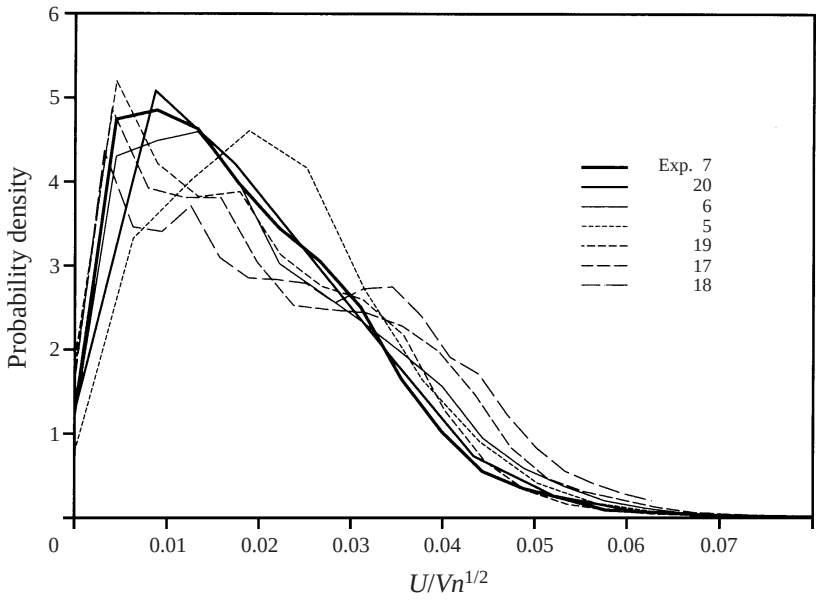

FIGURE 11. Probability density distribution of the velocity for the experiments listed in table 2. The measured velocities U are non-dimensionalized with $Vn^{1/2}$

expressed as

$$U_{max} = c_1 V n^{1/2} \quad c_1 = 0.061, \tag{5}$$

$$U_{rms} = c_2 V n^{1/2} \quad c_2 = 0.027. \tag{6}$$

The two quoted dimensionless proportionality constants are calculated from a least-squares fit to the data points of all experiments. The ratio of these constants indicates that U_{max} is approximately $2.2 \times U_{rms}$. Figure 11 shows that applying the scaling with $Vn^{1/2}$ makes the probability density distributions of the velocities in these experiments coincide, showing that the whole flow structure obeys this scaling. This indicates that the velocities U_{max} and U_{rms} used in the analysis above are good characteristics of the flow field.

Figure 12 presents information about the evolution of the vorticity averaged over the area of the central vortex, non-dimensionalized with the vorticity scale from the radius R and the maximum velocity U_{max} of the fully developed central vortex. The area of the central vortex was defined for this purpose as bounded by the mean-value steamfunction contour, which appropriately encompasses approximately 50% of the area within the forcing ring. The large gradients in the flow field at early times cause rather large errors in the calculations of the steamfunction and vorticity, and the data are not very accurate at these times. When the large-scale circulation is established, the evolution of the vorticity becomes smooth and it settles down to a more or less constant value after $Nt \approx 1800$. The experiments with 8 sources and 8 sinks (7 and 20) converge towards a single constant value of about 1.1, and the experiments with 16 sources and 8 sinks (5, 19, 17 and 18) converge towards a value that is only slightly higher. The dimensional values of the average vorticity in the final state in Exps. 19 and 17 are approximately the same as in the reference Exp. 7.

The diameter of the central vortex still increases in most experiments after the large-

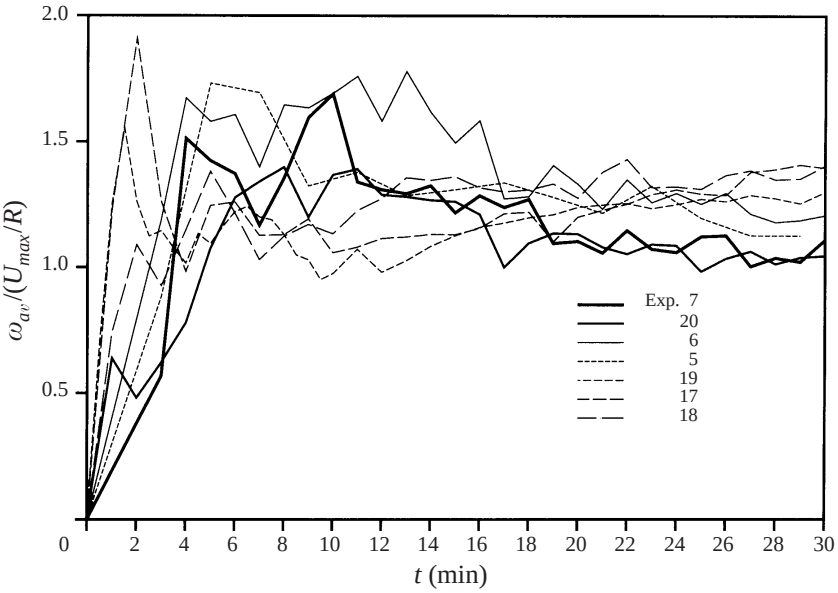

FIGURE 12. The non-dimensional average vorticity in the central vortex as a function of time for the 7 experimental runs listed in table 2.

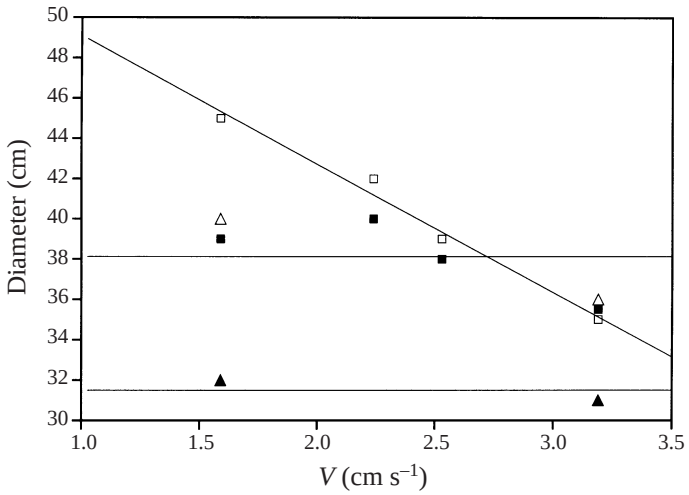

FIGURE 13. The diameter of the central vortex plotted against the forcing velocity V. Solid markers represent the diameter after 13 minutes forcing, with the horizontal lines indicating the average for forcing with 8 sources (triangles) and 16 sources (squares). Open markers represent the situation after 90 min forcing, and the sloping line is a best fit for the 4 experiments with 16 sources.

scale circulation first appears. This is indicated in figure 13 by the difference between the solid markers for the size at $t = 15$ min and the open markers for the size at $t = 90$ min. The diameter is defined as that of the streamline with the highest velocities along it. The initial diameter seems to be independent of the mean source velocity, and equal to 32 cm when $n = 8$, and 38 cm when $n = 16$. At later times, a stronger large-scale circulation squeezes the vortices linked to the sources more towards the forcing ring.

This results in a diameter of the central vortex that is only weakly dependent on the number of sources but that decreases with increasing source strength.

4.2. *Discussion*

In order to understand fully the different roles sources and sinks play in the transition to a state with a single large-scale circulation we examine their effects in more detail.

A sink only passively affects the flow field. The local flow field determines the fluid elements a sink removes, and therefore the vorticity it withdraws from the flow. This passive control over the vorticity flux explains the relatively small differences in the observed flow between the experiments 8 and 16 sinks. The only difference arises from the fact that in the experiment with the doubled number of sinks and unchanged number of sources (Exp. 6) the sinks are located closer to the sources. Extracting fluid at different locations causes the heads of the vortex strips from the sources to be slightly wider, but leaves the rest of the flow unchanged.

A source, on the other hand, actively controls the vorticity flux it creates. It injects new vorticity, independent of the flow field. The injected vorticity is determined by the velocity profile across the orifice and the shape of the orifice. In the present experiments this resulted in the production at each source of a three-dimensional ring of vorticity, collapsing into two planar strips of opposite vorticity, carrying the corresponding mass flux. These strips are of equal strength, giving zero circulation around a closed contour containing all the flow from the source. At the start of the forcing these strip pairs form a head in the shape of a vortex dipole. The dipoles interact with each other as they propagate into the interior of the domain. This was also observed by van Heijst & Flór (1989) for injections of finite duration. Owing to the continuous forcing in our experiments, vortex strips still emanate from the sources after the initial dipoles.

Doubling the number of sources obviously halves the distance between them. The vortex strips interact closer to the sources although, owing to the convergent geometry of the forcing ring, the interaction length is slightly more than half the original length. The earlier interaction decreases the maximum size of the dipole heads. The initial scale of the vortex structures is smaller, inducing more vortices on smaller scales, and the experiments with a large number of sources showed more vortices over a wider range of scales at the start (see figure 10). The vortices around the ring are, of course, affected by the sinks, which extract vorticity present near their location. We, therefore, observe in the experiments with a doubled number of sources, where there is no longer a sink present next to every source, alternating strong and weak vortices around the ring (see figure 10*b*). The later stages of the flow in the interior remain qualitatively unaffected by a larger number of sources and a large-scale circulation arises as before.

The early flow evolution shows a rapid increase in the average velocity (figure 8), and a more irregular, but still distinct, increase in vorticity (figure 12). The timescale of this spin-up is comparable to the circulation time of the established vortex, $T_c = \pi D/U_{max} \approx 3\,\mathrm{min}$. In this early spin-up phase, the velocities and vorticities in the experiment with 8 sources develop in a similar fashion to those in the experiment with 16 sources and an equal total energy flux, but when the velocities and vorticities reach a constant value at $Nt \approx 10^3$ the experiment with $n = 16$ and equal total momentum flux is closer to the reference experiment. So, it appears that initially the energy flux is the determining factor, whereas at later times it is the momentum flux that sets the strength of the circulation.

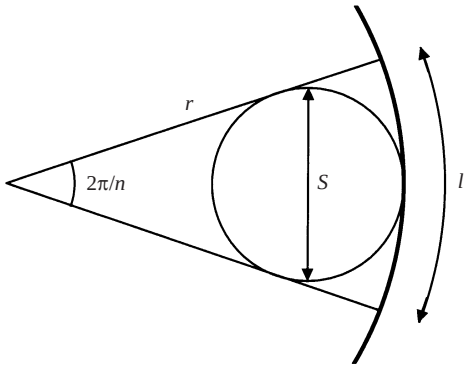

FIGURE 14. Sketch showing the definition of the effective source spacing S and the circumferential spacing l, depending on the number of sources n and the radius r.

The importance of the momentum flux can also be deduced from figure 9. When the energy in the flow field $E \propto U_{rms}^2$ has reached a constant value, the velocities in the field U_{rms} and U_{max} scale as $Vn^{1/2}$. This suggests two possible balances for the flow at this stage: either the total momentum flux from the n sources $M_{in} = Q\rho V \propto n\rho V^2$ is balanced by a momentum dissipation $M_{diss} \propto U_{rms}^2$, or the total two-dimensional vorticity flux from the sources $\sim nV^2$ is balanced by a dissipation of the circulation $\Gamma_{diss} \sim U_{rms}^2$. It is not yet understood why the momentum dissipation or circulation dissipation in the interior of the flow should scale in this manner.

The decrease in the values of the vorticity (as shown in figure 12) at much later times in Exps. 17 and 18 might be due to the increased amount of mixing by the strong source jets in those experiments. The values of the forcing parameter F_d, based on the diameter of the source orifices, are 6.9 and 8.9, respectively, and these high values are almost in the three-dimensional turbulance regime III as defined by Boubnov *et al.* (1994).

The size of the vortices around the forcing ring is set by the spacing of the sources. Linden *et al.* (1995) introduced the effective source spacing S as shown in figure 14. This maximum diameter of n structures that may be packed within the forcing ring of radius r can be written as

$$S = \frac{2\sin(\pi/n)}{1 + \sin(\pi/n)} r. \tag{7}$$

In the present experiments, $S = 15.6$ cm or $S = 9.2$ cm for 8 or 16 sources, respectively. In figure 15(*a*), 8 circles of the former diameter are drawn on the vorticity field of Exp. 7, 13 min after the start of the forcing. The actual size of the negative vortices is slightly smaller than those circles, since the narrow strips of positive vorticity are located between two sources as well. The area of the interior that is left over after the vortices bound to the sources have taken their space, sets the size of the large-scale circulation when it first arises. Therefore, it is only the number of the sources that determines the size of the central vortex in this early phase. The solid markers in figure 13 show that the initial central vortex size is approximately 32 cm for the case with 8 sources, and 38 cm for 16 sources, values which are consistent with (7).

At later times, however, the size seems to depend on the stength of the sources rather than their number. Visual observations indicate more vertical mixing, especially close to the sources, resulting in a less two-dimensional flow and more disperse vortex structures around the ring. The central vortex appears to have achieved a larger vertical

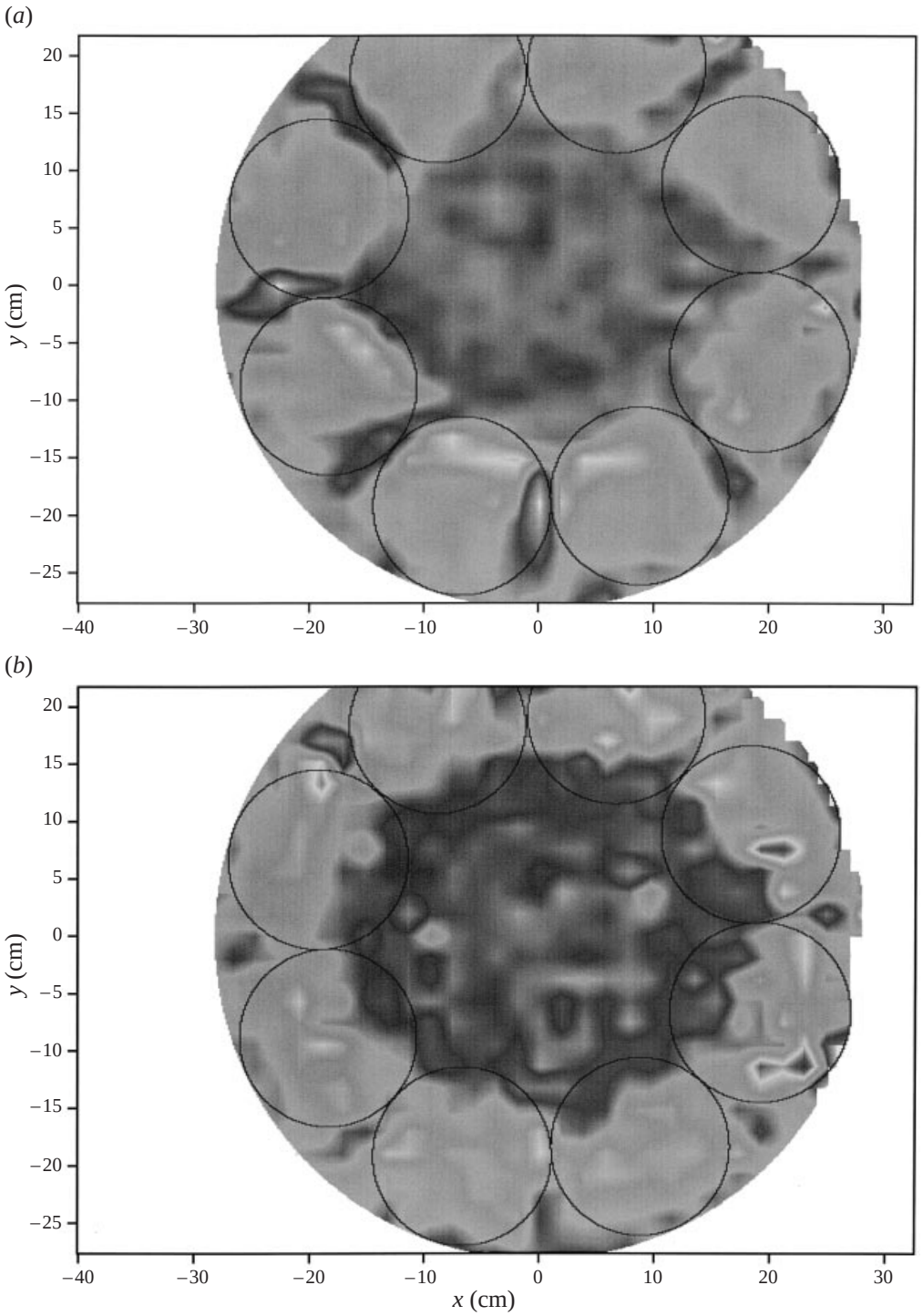

FIGURE 15. Circles indicating the maximum vortex size that can be packed within the forcing ring, drawn on the vorticity field of Exp. 7:8 sources, 8 sinks, $V = 3.2$ cm s^{-1}. (*a*) After 13 min, (*b*) after 90 min.

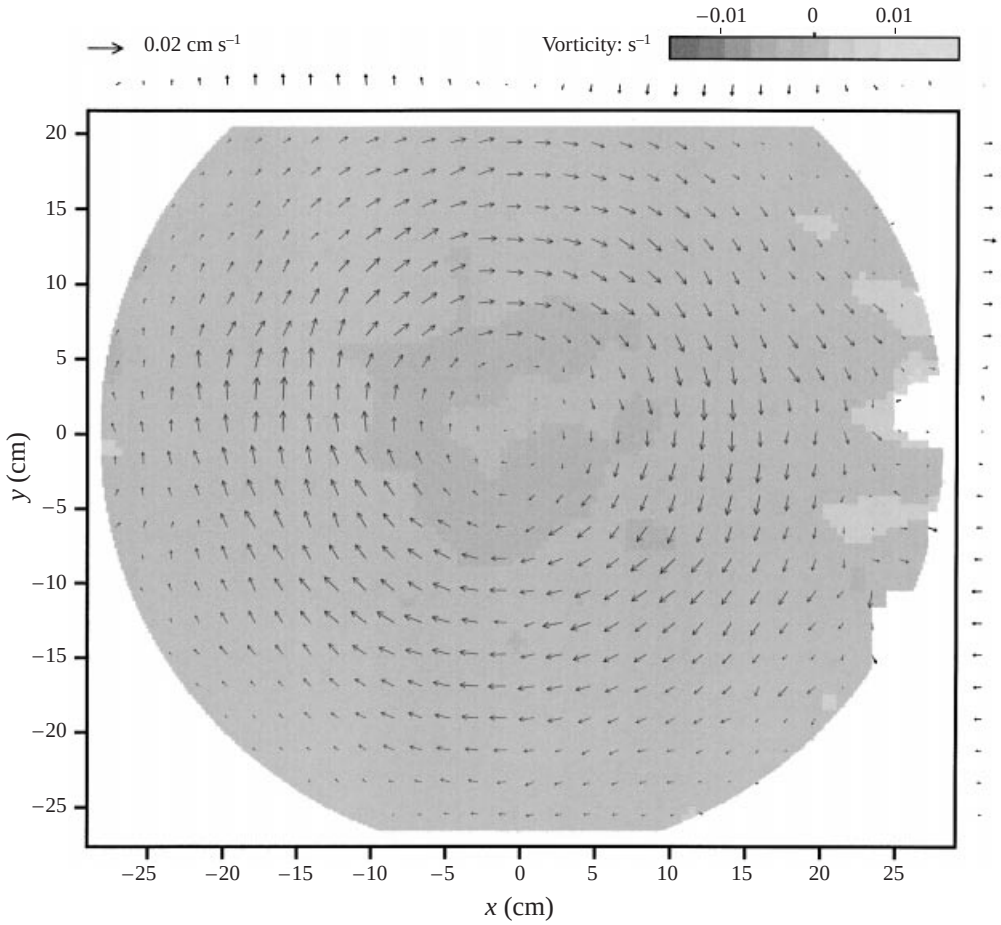

FIGURE 16. The initial perturbation flow field in Exp. 7*c*, time-averaged over 30 s just before the start of the experiment.

extent, perhaps even reaching the surface and bottom. Figure 15(*b*) shows that the central vortex has become stronger and has pushed the less well pronounced vortices connected with the individual sources to the side. The extent of the large-scale circulation decreases with increasing source velocities, as the open markers in figure 13 indicate.

5. Effects of an initial perturbation

5.1. *Observations of the direction of the large-scale circulation*

In each unperturbed experiment discussed above, the sense of rotation of the large-scale circulation, once it was fully developed, remained constant with time. The circulation was consistently anticlockwise in all experiments, as also noted by Linden *et al.* (1995), and is quite surprising, given the production of vortices of both signs by the sources. The suggestion that it might be related to some weak bias in the forcing mechanism was investigated by examining the effects of an initial perturbation on the flow.

The clockwise initial perturbations induced by the method described in § 2 were characterized by a weak, approximately constant, negative vorticity in the middle of the tank, extending to about 50% of the radius of the area in which measurements

were taken. Closer to the walls, weak positive vorticity was present. A typical perturbation velocity field is shown in figure 16. In experiments with a stronger perturbation the area of negative vorticity was somewhat larger, producing higher shear values close to the boundaries, especially near the middle of the walls of the square tank. For weaker perturbations the negative vorticity was not always spread out evenly, yeilding several local vorticity maxima. The decay of the perturbation was not studied in detail, but the experiments were started when the perturbation was adjudged to have the desired strength.

In the early stages of the flow with an initial perturbation (figure 17), the flow from the sources is deflected as soon as the flow has collapsed into planar motion, even though the initial clockwise background field cannot be seen using this velocity scale for the plot. With this clockwise initial flow, the deflection is to the left and, consequently, the positive part of the double vorticity strip emanating from each source rolls up into a vortex faster than the opposite vorticity. Thus, the positive vorticity becomes concentrated in a set of vortices around the ring, whereas the negative vorticity propagates into the interior to form a large clockwise central vortex. This growing large-scale circulation continues to entrain negative vorticity from the sources and becomes quasi-steady, with vorticity distributions opposite to those depicted in figure 4. The direction of rotation of the central vortex remained clockwise for the remainder of the experiment (200 min) and it appeared that it could remain so indefinitely.

Figure 18 shows the evolution of an experiment identical to that shown in figure 17 but where the intial clockwise perturbation was weaker and the final circulation was eventually anticlockwise. In the first minutes after the start of the forcing, a slight deflection of the source jets is observed, resulting in a minimal dominance of negative vorticity in the interior. However, as time progresses, the jets exhibit an increasing preference for producing more concentrate negative vortices at the outer boundary, leaving the positive vorticity to propagate into the interior of the tank. It is only at 10 min after the start of the forcing that the positive vorticity dominates the central area. The anticlockwise final circulation attains its usual axisymmetric state some 5 min later.

In total, 12 experiments with initial perturbations of different strengths were analysed in detail. Two characteristics of the initial flow, the r.m.s. velocity U_{rms} in the whole field, and the vorticity averaged over the area within the streamline with $\psi = 0$, were evaluated. The results showed that the direction of the final circulation, as set-up by the forcing, reverses at a clockwise initial circulation with an average vorticity of approximately -10^{-3} s^{-1}. This critical vorticity is about 4% of the average vorticity in the final circulation. The corresponding r.m.s. velocity in the initial field is roughly a tenth of the r.m.s. velocity in the final circulation, and two orders of magnitude smaller than the mean source jet velocity.

5.2. *Discussion*

It is very unlikely that the strikingly consistent feature of an anticlockwise (cyclonic) large-scale circulation is caused by the rotation of the Earth. Values of the Rossby-number $Ro = V/fl$ of about 10^3 indicate that intertial forces are far stronger than the Coriolis forces. Further, the timescale for the onset of the circulation is much less than a day, so rotational effects do not account for the observed asymmetry.

The above experiments show that a relatively small initial circulation causes a deflection of the source jets during the early evolution of the flow, which causes more concentrated vortices of one sign to be produced at the sources (figure 17). Thus, a small initial perturbation can determine the direction of the final circulation. When the large-scale circulation is established, it deflects the source jets further in such a

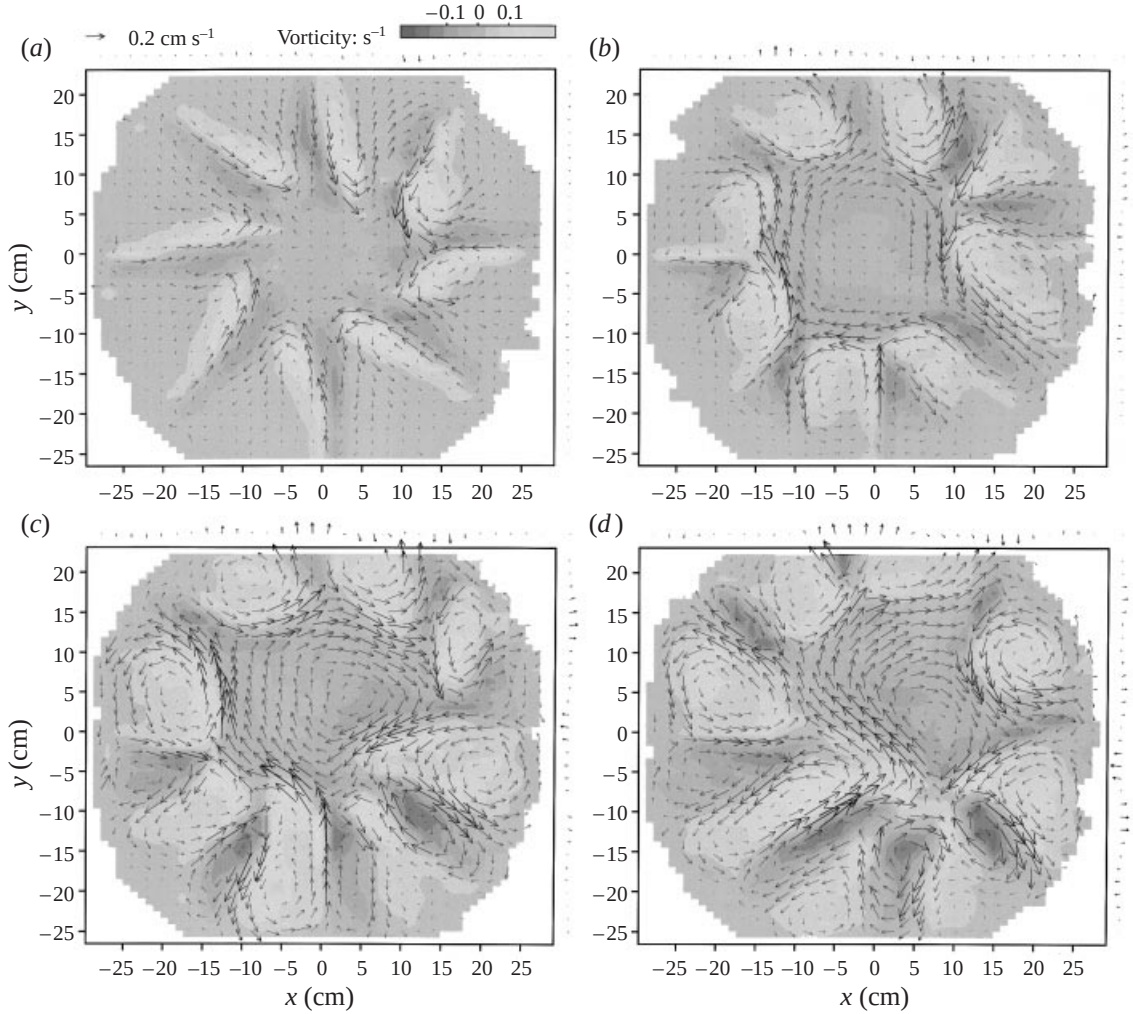

FIGURE 17. Velocity (arrows) and vorticity (shading) fields in experiment 8*b*, at 1, 2, 3 and 4 min after the start of the forcing. The forcing was identical to that in Exp. 7 (figure 2), but a small clockwise initial flow was induced before the forcing was turned on.

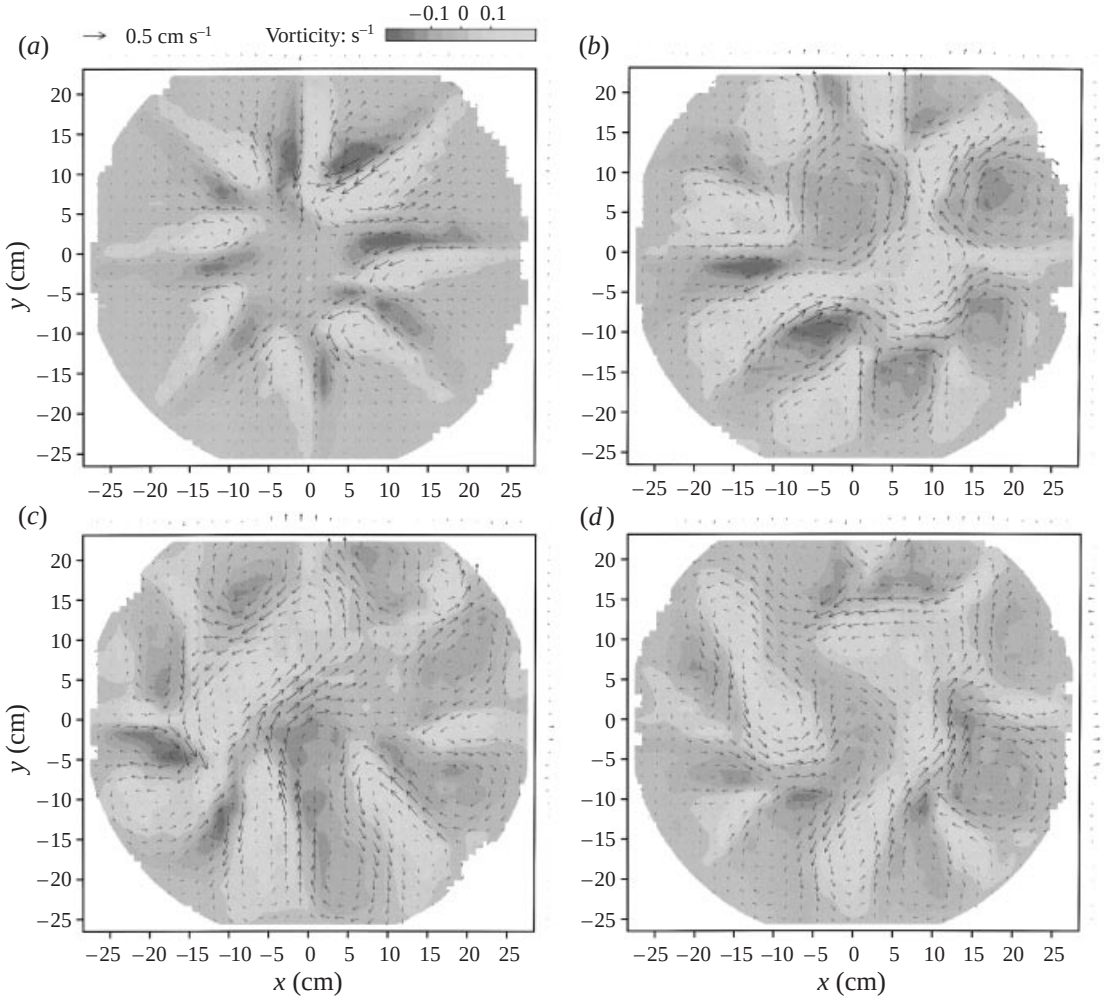

FIGURE 18. Velocity (arrows) and vorticity (shading) fields in Exp. 8, at 1, 3, 5 and 9 min after the start of the forcing. The forcing was identical to that in Exp. 7 (figure 2). A small clockwise initial flow was induced before the forcing was turned on, but this was weaker than in Exp. 8*b* (figure 17).

way as to enhance its circulation. This positive feedback makes it difficult for the circulation to reverse its direction.

When the initial perturbation is sufficiently weak, the final circulation can reverse it (Exps. 8 and 7*d*, figure 18). In the early stages, the jets are not deflected sufficiently to create a dominant circulation in the same direction as the perturbation. The feedback is weak and the jets revert to their usual preference for creating clockwise vortices at the ring, setting up an anticlockwise circulation in the interior. In this case, it does takes longer for the single central circulation to develop. In one experiment (Exp. 16, not included in the further analysis), two large opposing vortices persisted in the interior for a long time: approximately 45 min. The strength of the (unintended) initial perturbation was comparable to that in Exp. 18, but was not as smooth as the one in figure 16, and was probably the cause of the development of two strong vortices in the middle.

Detailed further analysis of those experiments thought to have zero initial flow revealed that in most cases some net positive vorticity was present before the start of the forcing (Exps. 5, 17, 18, 19 and 20). This tiny initial perturbation has most probably contributed to the direction of the final circulation. In the cases where no net initial circulation seemed to be present (Exps. 6 and 7), diffuse patches of vorticity near the sources, too weak to be mesured in the present experimental set-up, may have caused small deflections as well.

Nevertheless, the fact that the large-scale circulation changes direction at a finite negative initial circulation, indicates a preference for an anticlockwise circulation, which might arise from a small consistent bias in the forcing mechanism. A slight non-radial offset in the direction of the sources will favour concentrated vortices of one sign, but, apparently, this effect can be overcome by an initial circulation above a certain low threshold. The ratio of the critical initial perturbation velocity to the jet velocity is 10^{-2}. Assuming that at the threshold the tangential component of the jet velocity balances the critical perturbation velocity, this would suggest a directional offset of 0.6°. Such offsets are smaller than the machined tolerance of the radial direction of the sources.

6. Decaying circulation

6.1. *Observations*

Before the forcing was switched off, the flow field typically looked like figure 2(*d*), with a strong vortex in the middle, surrounded by 8 or 16 smaller concentrated vortices, depending on the number of sources. When the forcing ceased, the motion slowly decayed and here we report on this spin-down of the system.

Small inequalities in the source stengths, or even disconnected source–sink pairs, lead to a large-scale circulation which was not perfectly axisymmetric at the start of spin-down, but rather elliptical, egg-shaped or almost triangular in shape. Figure 19 provides an example of the vorticity distribution in the decaying circulation. This egg-shaped structure rotated very slowly in the same sense as its circulation. The revolution time was approximately 17 min, or eight times the circulation time, defined as $T_C = 2\pi/\omega_{av}$ where ω_{av} is the average vorticity in the central vortex. As can be seen in figure 20, the aspect ratio of the vortex increases immediately after the forcing was switched off, but then the vortex becomes more circular as it decays. The aspect ratios of both the streamlines and the vorticity contours oscillate, and the amplitude of the oscillation is approximately twice the uncertainty in the calculation of the aspect ratio. The oscillations in the two aspect ratios are out of phase, as can be seen

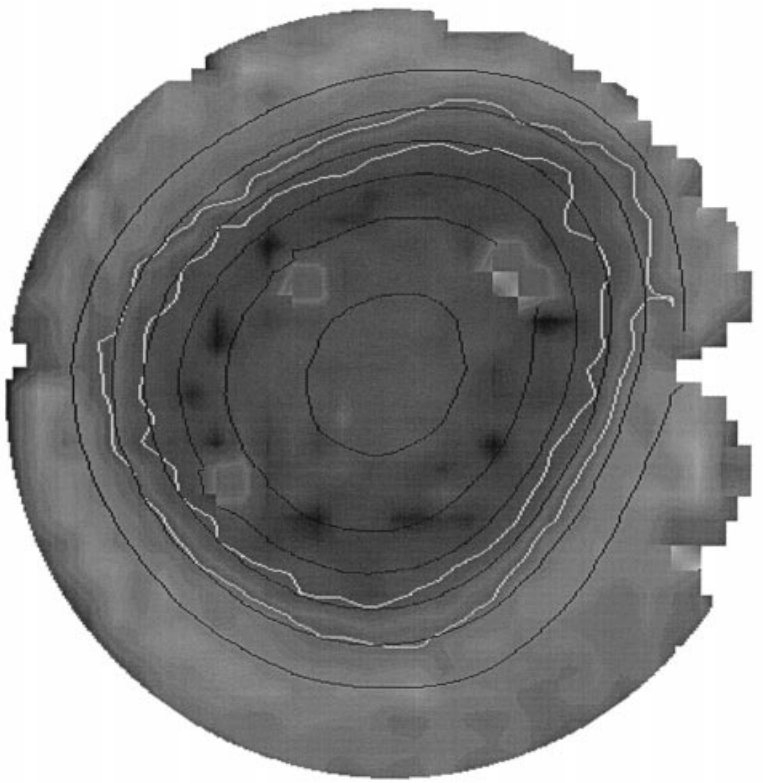

FIGURE 19. Streamlines (black lines) and vorticity field (shading and white lines) of the decaying vortex in Exp. 17, 4 min after switching off the forcing.

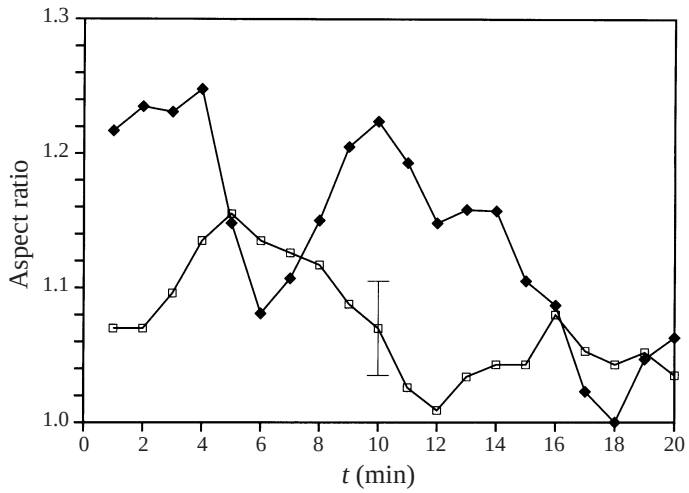

FIGURE 20. The aspect ratio of □, streamlines and ◆, vorticity contours in the decaying central vortex in Exp. 17. The indicated time is measured from the moment the forcing was switched off. One error bar is drawn to give an idea of the uncertainty in the aspect ratio.

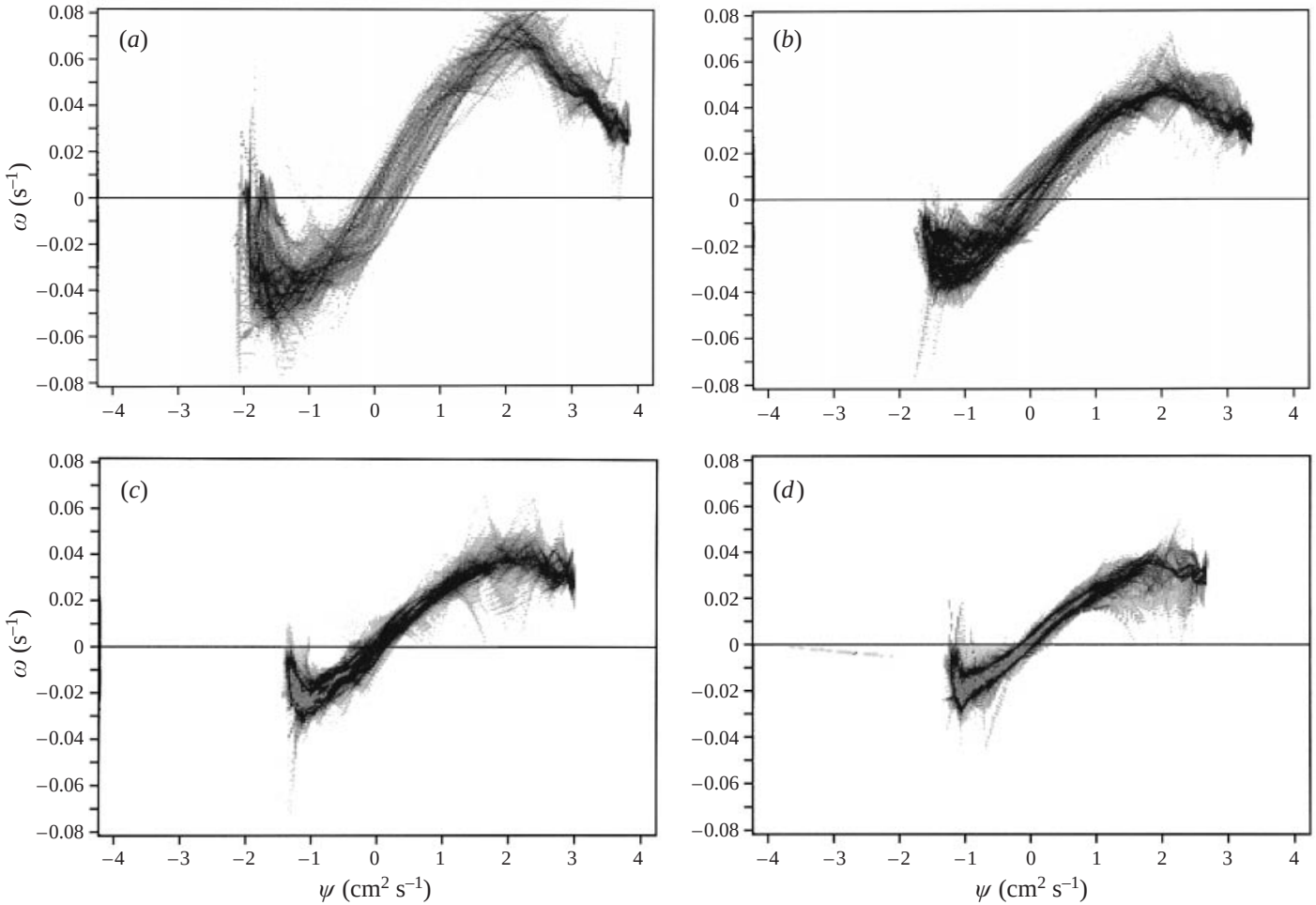

FIGURE 21. (ω, ψ) scatter plots of the decaying vorticity field in Exp. 17, at (*a*) 1 min, (*b*) 5 min, (*c*) 10 min, and (*d*) 15 min after switching off the forcing. The (ω, ψ)-values of all points on a grid in physical space, with a mesh size of approximately $(1\,\mathrm{mm})^2$, are plotted.

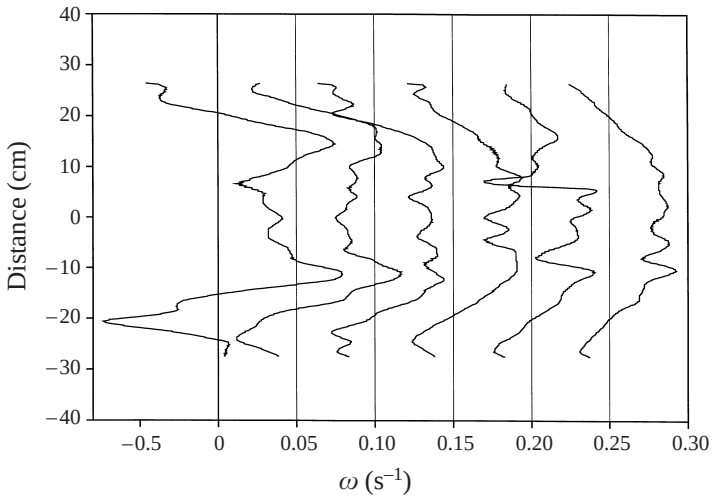

FIGURE 22. Cross-sections of the vorticity field in the decaying vortex. Curves represent the vorticities along the line $y = 2x$ (with x and y as in figure 3) at 1, 4, 8, 12, 16 and 20 min after switching off the forcing. Each curve is shifted horizontally over 0.05 s^{-1} with respect to the previous curve.

in figure 20. The shape of the vortex does not differ significantly from a circle after around 8 circulation times T_C, or approximately one revolution of the structure.

Figure 19 also shows five streamfunction contours and two vorticity contours in the vortex. The vorticity contours form somewhat more elongated ellipses than the smooth streamfunction contours. This slight misalignment indicates that the function $\omega(\psi)$ is not single-valued, as can bee seen in figure 21, which shows scatter plots in the (ω, ψ)-plane at several times during the decay. These plots are similar to the (ω, ψ) scatter plots shown in figure 5. Again, decreasing ψ can be interpreted as increasing radius, with maximum values of ψ in the middle of the vortex.

Initially, the vorticity has its maximum value around the edge of the vortex, as pointed out earlier. In the middle, where ψ is maximal, the vorticity can be 50% lower. As the maximum value of the vorticity decreases, the vorticity in the patch becomes more homogeneous: a plateau of constant vorticity emerges. The vorticity gradients flatten out and at later times the interior of the vortex performs a solid-body rotation, slowly decaying in time. The largest amount of scatter occurs for negative values of ψ, indicating the wide range of vorticities around the outer ring. During the decay the amount of scatter diminishes quickly and the scatter plots collapse as time progresses.

The evolution of a cross-section of the vorticity field can be seen in figure 22. This figure shows that the vorticity maxima at the edge of the central vortex decay very quickly, and have disappeared altogether after 10 min. This leaves a very slowly decaying vortex with homogeneously distributed vorticity and with a constant horizontal extent. The smaller vorticity structures around the edge of the domain decay relatively quickly: after 10 min the vorticity in this outer region is reduced to approximately half the initial value. Their horizontal extent is much smaller than that of the central vortex, and visual observations suggest that their vertical extent is also smaller. These structures have disappeared as self-contained entities when the central vortex reaches an axisymmetric state, and only a band of weak opposite vorticity remains.

The evolution of the vorticity averaged over the central vortex, defined as the area

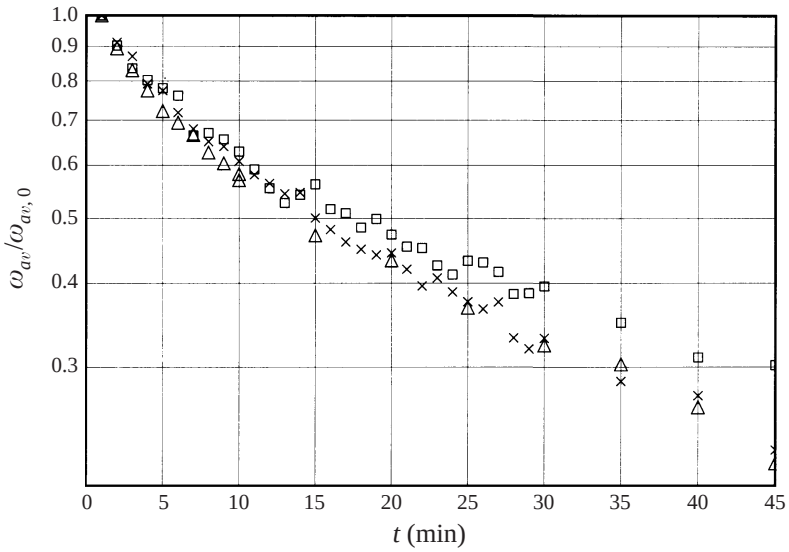

FIGURE 23. The evolution of the average vorticity in the central vortex, normalized with its value at the moment the forcing was turned off. ×, Exp. 17, □, Exp. 18, △, Exp. 19.

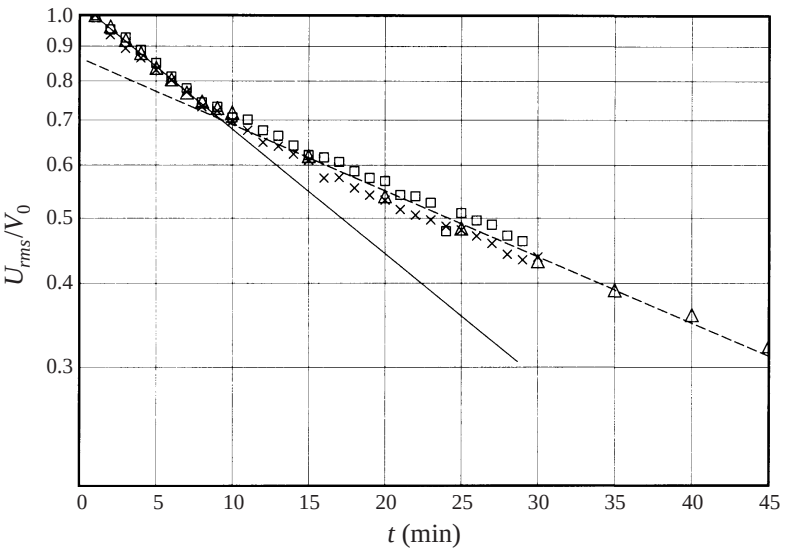

FIGURE 24. The non-dimensionalized r.m.s velocity of the total flow field plotted versus time for the decaying vortex in ×, Exp. 17, □, Exp. 18, △, Exp. 19. Plotted lines are exponential fits to the data for $t < 8$ min and 10 min $< t < 45$ min, with characteristic decay times of 23 min and 44 min, respectively.

within the streamline with $\psi = 0$, is shown on a semi-logarithmic plot in figure 23. At first, the characteristic decay time is 12 min, but the decay slows down after 5 min to a characteristic time of about 45 min. Figure 24 displays the decay of the r.m.s. velocities, averaged over the whole field. Similar remarks can be made here: the initial fast decay slows down after 5–10 min to a decay timescale of approximately 45 min.

6.2. *Discussion*

The scatter plots in the (ω, ψ)-plane of the unforced motion (figure 21) show considerable variability immediately after the forcing is switched off, especially at low values of the streamfunction. As the negative vortices linked to the sources decay, the amount of scatter is quickly reduced. The central vortex adjusts itself to the decay of the forcing vortices and its aspect ratio is observed to approach unity at large times. This axisymmetrization of the freely evolving vortex is probably due to a process described by Melander, McWilliams & Zabusky (1987). They argue that this process is essentially inviscid and takes place via vortex filamentation resulting from a misalignment of streamfunction and vorticity contours. A slight mismatch was indeed observed in the early stages of the decay (see figure 19), but our spatial resolution was too coarse to observe any possible filamentation. Another aspect of their numerical simulations was an oscillation of the aspect ratio of the vorticity contours after an initial rapid decay, whereas the aspect ratio of the streamlines tended towards one without similar flutuations. In the present experiments, the aspect ratio of streamlines seems to oscillate, but the data are not accurate enough to distinguish clearly between monotonous decay and fluctuating behaviour. The aspect ratio of vorticity contours could not be measured accurately. Further experiments are needed to yield more accurate information about the oscillation frequency and the decay rate of the aspect ratio.

In the experiments, the decaying central vortex not only becomes axisymmetric, but also settles in the middle of the tank. Recent numerical simulations by van Geffen, Meleshko & van Heijst (1996) showed that a weakly dissipative two-dimensional monopolar vortex will only slowly become closer to the centre in a bounded rectangular domain. However, when no-slip instead of free-slip boundary conditions are imposed, the opposite vorticity induced near the walls causes the vortex to move quickly to the centre of the domain. Their numerical simulations showed that the path is not completely smooth, but kinks appear in the trajectory. This could not be observed in our experiments, since the vortex was quite close to the middle when the forcing was switched off.

The (ω, ψ)-values for the large vortex in the middle collapse onto a single curve within a few minutes, mirroring the more two-dimensional and quasi-static behaviour of the flow. Horizontal viscous difffusion reduces gradients in the vorticity and the curve becomes almost a straight line. This linear relationship between ω and ψ is similar to that found by Kloosterziel & van Heijst (1991) for monopolar vortices in a rotating fluid. Flór & van Heijst (1994) also observed a linearization of the ω–ψ relation, for circular as well as square domains, and with forcing by a moving rake as well as forcing by jets. This linearization process was described by van de Konijnenberg (1995) in mathematical terms as an evolution towards the lowest eigenmode of the system, owing to horizontal viscous diffusion.

The Ekman timescale $T_E = H(\nu\omega)^{-1/2}$ for the decay of vorticity in the central vortex is 18 min, when calculated using a characteristic average initial vorticity of $0.04\,\mathrm{s}^{-1}$. This decay time is very close to that measured in the experiments. However, the spin-down process on which this decay time is based involves Ekman pumping, which is inhibited by the stratification, as pointed out by Barcilon & Pedlosky (1967). Integrating the continuity equation in the Ekman layer from $z = 0$ to $z \gg \delta_E = (\nu/\Omega)^{1/2}$, we obtain the Ekman pumping velocity W_G in the geostrophic interior as a function of the vertical component ω_G of the vorticity in the flow away from the boundary layer: $w_G = \frac{1}{2}\delta_E\omega_G$. Dimensional analysis of the relevant quantities shows

that the height that a fluid parcel with velocity w_G can be raised may be estimated by

$$h \approx \frac{w_G}{N} = \frac{\delta_E \omega_G}{2N}, \tag{8}$$

which evaluates to $h \approx 0.03\,\text{cm} \ll H$ for the present experiments. The typical timescale for this is $2\pi N \approx 6s$. This shows that Ekman pumping might only play a role at the very early stages of spin-down in a stratified fluid. At later times, only dissipation by viscous effects and by radiation of internal gravity waves can account for the spin-down of the vortex.

The timescale for decay by vertical viscosity from the bottom of the tank is $T_{visc} = H^2/\nu\pi^2 \approx 75\,\text{min}$, which is much slower than spin-down by Ekman pumping. The timescale for the initial decay of vorticity and r.m.s. velocity that was measured in the experiments was only about 12 min, which suggests a vertical scale of only 3 cm. Therefore vertical diffusion alone cannot account for the fast decay, and lateral viscosity must play an additional role. During the initial decay, the vorticity changes from its maximum to its minimum over approximately 6 cm at the edge of the vortex. This gives a typical horizontal lengthscale of 3 cm, which accounts for the decay timescale of 12 min. Figure 22 shows that the large gradients disappear over that timescale.

At later times, lateral viscosity from the sidewalls of the tank might play a role in the decay, although at a slower rate owing to the longer horizontal lengthscale. The decay time can be estimated by solving the vorticity equation for axisymmetric viscous decay in a domain with radius R. Applying the boundary conditions of zero vorticity on the bottom and sidewalls, and $\partial\omega/\partial z = 0$ at mid-depth $z = \frac{1}{2}H$ yields

$$T'_{visc} = \frac{H^2/\nu\pi^2}{(2m+1)^2 + \left(\dfrac{\alpha_n}{\pi}\dfrac{H}{R}\right)^2}. \tag{9}$$

Here m is the vertical mode number and α_n is the nth zero of the Bessel function J_o where n determines the radial mode. The square shape of the tank did not seem to be important in the experiments, since the fluid in the corners is stationary. In the experiments, the ratio $H/R = 2\sqrt{3}$ and from (9) we find a reduction of the decay time by 21% for the lowest vertical and radial mode ($m = 0$, $n = 1$) owing to the addition of horizontal diffusion. For the next radial mode ($n = 2$), with a ring of opposite vorticity around the central vortex, the reduction is 58%, yielding a decay time of 31 min. These decay times are comparable with the observed decay timescale at later times of approximately 44 min (seen figures 23 and 24).

In the experiments, some motion was observed at the surface, but further quantitative information on the actual vertical profile is not available and the effect of vertical shear on the decay is uncertain. Further experiments with different fluid depths H and velocity measurements at several levels are necessary to understand fully the spin-down of the vortex.

7. Conclusions

The experiments in a stratified fluid, forced with radially directed sources and sinks in a horizontal plane, showed the development of a turbulent flow field that is planar to a good approximation. Coherent vortex structures appear and an inverse energy

cascade is observed: vortices grow by the merging of vortices of like sign. The planar flow finally self-organizes into a single vortex structure of the largest available scale, while the influence of the individual sources and sinks is restricted to a small area with vortices close to the forcing.

The central vortex has a homogeneous vorticity distribution in its centre, with higher vorticities at the edge. Together with the opposite vorticity outside the central vortex this gives a barrier with high velocity shear, that is observed to shield the central vortex from the opposite vorticity produced by the sources. However, patches of like-sign vorticity from the exterior do cross this barrier and their intermittent entrainment maintains the central vortex against decay. Patches of opposite vorticity, and patches of vorticity lower than the mean value in the central vortex, are observed to be expelled intermittently. The (ω, ψ)-diagnostics showed that, at later times, the net influx of vorticity is comparable with the decay resulting from vertical diffusion of momentum, and the flow reaches a quasi-steady state. We expect these processes to be relevant in the spin-down process.

Changing the number of sinks does not affect the flow, since they only passively extract fluid, whereas the sources always produce vorticity. The number of sources sets the size of the forcing vortices and thereby the space available for the central vortex, although the formal level of rotational symmetry of the flow is set by the smallest of the number of sources and the number of sinks. At later stages of the flow, the strength of the source jets affects the size of the vortex: for weaker forcing, the central vortex pushes the forcing vortices aside. In the final state, the velocities in the flow are observed to scale with strength of the forcing multiplied by the square root of the number of sources, $Vn^{1/2}$. The total flux of momentum from the sources seems to balance an overall momentum dissipation proportional to U_{rms}^2.

The present experimental apparatus showed a small bias towards an anticlockwise vortex. This can be offset by an initial clockwise flow of about 1% of the strength of the final circulation, which suggests that the offset in the direction of the sources is of order 1°. The sense of the circulation once set, either by the initial perturbation or the bias in the sources, remains constant thereafter.

Once the forcing is switched off, the vortex spins down and becomes axisymmetric owing to a non-viscous process. During the axisymmetrization, its aspect ratio oscillates. Streamlines and isovorticity contours coincide and the $\omega(\psi)$-relation becomes linear on a timescale of approximately 20 min. The decay of the vorticity is much faster than can be accounted for by vertical viscous diffusion alone. Horizontal viscous diffusion plays an important additional role. The fast initial decay is an effect of the short horizontal scale of the band of high vorticity around the vortex, and the decay is slower in later stages owing to the larger scale of the vortex as a whole. Little information is available for the present experiments about the vertical structure of the flow. We are currently planning new experiments with velocity measurements at several levels, which we hope will help to understand the spin-down of a vortex in a stratified fluid.

This work was carried out while FdR was in Cambridge on an ERASMUS exchange project from Eindhoven University of Technology. The support of Professor G. J. F. van Heijst and the financial assistance from the European Union for this project are gratefully acknowledged. The research was also supported by the Natural Environment Research Council (Grant GR3/10488).

REFERENCES

Barcilon, V. & Pedlosky, J. 1967 Linear theory of rotating stratified fluid motions. *J. Fluid Mech.* **29**, 1–16.

Boubnov, B. M., Dalziel, S. B. & Linden, P. F. 1994 source–sink turbulence in a stratified fluid. *J. Fluid Mech.* **261**, 273–303.

Dalziel, S. B. 1992 Decay of rotating turbulence: some particle tracking experiments. *Appl. Sci. Res.* **49**, 217–244.

Dalziel, S. B. 1993 Rayleigh–Taylor instability: experiments with image analysis. *Dyn. Atmos. Oceans* **20**, 127–153.

Dalziel, S. B., Linden, P. F. & Boubnov, B. M. 1996 Experiments on turbulence in stratified rotating flows. In *Waves and Nonlinear Processes in Hydrodynamics* (ed. Grue, Gjevik & Weber), pp. 317–330. Kluwer.

Dritschel, D. G., Haynes, P. H. & McIntyre, M. E. 1998 Permeability of the stratospheric vortex edge: vortex scattering experiments. Submitted to *Nature*.

Fincham, A. M., Maxworthy, T. & Spedding, G. R. 1996 Energy dissipation and vortex structure in freely decaying, stratified turbulence. *Dyn. Atmos Oceans* **23**, 155–169.

Flór, J.-B. & Heijst, G. J. F. van 1994 An experimental study on dipolar structures in a stratified fluid. *J. Fluid Mech.* **279**, 101–133.

Flór, J.-B. & Heijst, G. J. F. van 1996 Stable and unstable monopolar vortices in a stratified fluid. *J. Fluid Mech.* **311**, 257–287.

Geffen, J. H. G. M. van., Meleshko, V. V. & Heijst, G. J. F. van 1996 Motion of a two-dimensional monopolar vortex in a bounded rectangular domain. *Phys. Fluids* **8**, 2393–2399.

Heijst, G. J. F. van & Flór, J.-B. 1989 Dipole formation and collisions in a stratified fluid. *Nature* **340**, 212–215.

Kloosterziel, R. C. & Heijst, G. J. F. van 1991 An experimental study of unstable barotropic vortices in a rotating fluid. *J. Fluid Mech.* **223**, 1–24.

Konijnenberg, J. A. van de 1995 Spin-up in non-axisymmetric containers. PhD thesis, Eindhoven University of Technology.

Legras, B., Santangelo, P. & Benzi, R. 1988 High resolution numerical experiments for forced two-dimensional turbulence. *Europhys. Lett.* **5**, 37–42.

Linden, P. F., Boubnov, B. M. & Dalziel, S. B. 1995 Source–sink turbulence in a rotating, stratified fluid. *J. Fluid Mech.* **298**, 81–112.

McWilliams, J. C. 1984 The emergence of isolated coherent vortices in turbulent flow. *J. Fluid Mech.* **146**, 21–43.

Melander, M. V., McWilliams, J. C. & Zabusky, N. J. 1987 Axisymmetrization and vorticity-gradient intensification of an isolated two-dimensional vortex through filamentation. *J. Fluid Mech.* **178**, 137–159.

Narimousa, N., Maxworthy, T. & Spedding, G. R. 1991 Experiments on the structure and dynamics of forced, quasi-two-dimensional turbulence. *J. Fluid Mech.* **223**, 113–133.

Norton, W. A. 1994 Breaking Rossby waves in a model stratosphere diagnosed by a vortex-following coordinate system and a technique for advecting material contours. *J. Atmos. Sci.* **51**, 654–673.

Read, P. L., Rhines, P. B. & White, A. A. 1986 Geostrophic scatter diagrams and potential vorticity dynamics. *J. Atm. Sci.* **43**, 3226–3240.

Sommeria, J. 1986 Experimental study of the two-dimensional inverse energy cascade in a square box. *J. Fluid Mech.* **170**, 139–168.

Voropayev, S. I. & Afanasyev, Y. D. 1994 *Vortex Structures in a Stratified Fluid*. London: Chapman & Hall.

Yap, C. T. & Van Atta, C. W. 1993 Experimental studies of the development of quasi-two-dimensional turbulence in stably stratified fluid. *Dyn. Atmos. Oceans* **19**, 289–323.